piRNA-guided co-transcriptional silencing coopts nuclear export factors

Martin H. Fabry,[1,*] Filippo Ciabrelli,[1,*] Marzia Munafò,[1,*] Evelyn L. Eastwood,[1] Emma Kneuss,[1] Ilaria Falciatori,[1] Federica A. Falconio,[1] Gregory J. Hannon,[1,#] Benjamin Czech[1,#]

[1]Cancer Research UK Cambridge Institute
University of Cambridge
Li Ka Shing Centre
Cambridge CB2 0RE
United Kingdom

* These authors contributed equally

[#] Correspondence: greg.hannon@cruk.cam.ac.uk (G.J.H.)
benjamin.czech@cruk.cam.ac.uk (B.C.)

Abstract

The PIWI-interacting RNA (piRNA) pathway is a small RNA-based immune system that controls the expression of transposons and maintains genome integrity in animal gonads. In *Drosophila*, piRNA-guided silencing is achieved, in part, via co-transcriptional repression of transposons by Piwi. This depends on Panoramix (Panx); however, precisely how an RNA binding event silences transcription remains to be determined. Here we show that Nuclear Export Factor 2 (Nxf2) and its co-factor, Nxt1, form a complex with Panx and are required for co-transcriptional silencing of transposons in somatic and germline cells of the ovary. Tethering of Nxf2 or Nxt1 to RNA results in silencing of target loci and the concomitant accumulation of repressive chromatin marks. Nxf2 and Panx proteins are mutually required for proper localization and stability. We mapped the protein domains crucial for the Nxf2/Panx complex formation and show that the amino-terminal portion of Panx is sufficient to induce transcriptional silencing.

Introduction

The piRNA pathway is a small RNA-based immune system that represses transposable elements in animal gonadal tissues (Czech et al., 2018; Ozata et al., 2019). At the core of this pathway are PIWI-clade Argonaute proteins that are guided by 23-30nt piRNA partners to silence transposon targets via two main mechanisms. In *Drosophila,* Aubergine and Argonaute3 enforce post-transcriptional gene silencing (PTGS) via direct cleavage of transposon mRNAs in the cytoplasm (Brennecke et al., 2007; Gunawardane et al., 2007). Piwi, in contrast, operates in the nucleus where it instructs the co-transcriptional gene silencing (TGS) of transposon insertions (Brennecke et al., 2007; Klenov et al., 2011; Sienski et al., 2012). Mutations that compromise TGS result in severe loss of transposon control, despite normal piRNA levels (Donertas et al., 2013; Le Thomas et al., 2013; Muerdter et al., 2013; Ohtani et al., 2013; Rozhkov et al., 2013; Sienski et al., 2015; Sienski et al., 2012; Yu et al., 2015).

Piwi, in complex with piRNAs, detects nascent transposon RNAs arising from active insertions and directs the silencing of these loci. Target silencing is achieved via recruitment of histone modifying enzymes that deposit repressive chromatin marks, mainly trimethylation of Lysine 9 on Histone 3 (H3K9me3) (Iwasaki et al., 2016; Klenov et al., 2014; Le Thomas et al., 2013; Rozhkov et al., 2013; Sienski et al., 2012; Wang and Elgin, 2011). Panoramix (Panx) is a key TGS effector, acting downstream of Piwi at the interface between the piRNA pathway and the general chromatin silencing machinery (Sienski et al., 2015; Yu et al., 2015). Strikingly, RNA-mediated recruitment of Panx, but not Piwi, to a locus is sufficient to trigger its epigenetic silencing, thus placing Panx at a critical node of the TGS mechanism. Downstream of Panx, the concerted action of dLsd1/Su(var)3-3 and Eggless/dSETDB1 erases H3K4me2 and concomitantly deposits H3K9me3, followed by chromatin compaction via Heterochromatin Protein 1a (HP1a/Su(var)205) (Czech et al., 2013; Iwasaki et al., 2016; Rangan et al., 2011; Sienski et al., 2015; Wang and Elgin, 2011; Yu et al., 2015). Precisely how Panx recruits these histone modifying enzymes and what other factors participate in this process remains an outstanding question.

Here we show that Panx coopts elements of the nuclear RNA export machinery to trigger transcriptional silencing. Panx is part of a complex that also contains Nuclear Export Factor 2 (Nxf2) and Nxt1/p15. Panx and Nxf2 are interdependent for their protein stability. *nxf2* mutants show strong de-repression of Piwi-regulated transposons and severe loss of H3K9me3 at affected loci, similarly to *panx* mutants. We find that the amino-terminus of Panx delivers the critical silencing signal, as it is necessary and sufficient to trigger the deposition of repressive chromatin marks if tethered to a reporter construct, while its carboxyl-terminal region is involved in the interaction with Nxf2. Nxf2 is closely related to the mRNA export factor Nxf1, which also interacts and functions with Nxt1 (Fribourg et al., 2001; Herold et al., 2001; Herold et al., 2000). Thus, our findings reveal that the evolution of transposon defense mechanisms involved exaptation of the nuclear RNA export machinery.

106
107

Results

Nxf2 is a TGS factor that interacts with Panx

To identify proteins associated with Panx, we immunoprecipitated a GFP-Panx fusion protein expressed from its endogenous promoter ((Handler et al., 2013); Figure 1—figure supplement 1A) from ovary lysates and identified co-purifying proteins by quantitative mass spectrometry. Three proteins showed the strongest enrichment and significance: Panx, Nxf2 and Nxt1 (Figure 1A, Figure 1-Source Data 1). Nxf2 is a homolog of the general messenger RNA (mRNA) export factor Nxf1 but was reported previously as being dispensable for canonical mRNA transport in S2 cells (Herold et al., 2001; Herold et al., 2003). Nxf2 contains all domains present in the family defined by Nxf1, namely an amino-terminal region (NTR), an RNA-binding domain (RBD), leucine-rich repeats (LRR), the NTF2-like domain (NTF2) and a Ubiquitin-associated (UBA) domain (Figure 1B and Figure 1—figure supplement 1B) (Herold et al., 2001). While the NTR, LRRs and RBD are typically involved in cargo binding, the NTF2 and UBA domains mediate binding to the Nuclear Pore Complex (NPC) and are required for Nxf1-mediated RNA export (Braun et al., 2001; Fribourg et al., 2001). Nxt1, also known as p15, is a co-factor of Nxf1 responsible for interaction with the NPC, specifically through the NTF2-fold (Fribourg et al., 2001; Levesque et al., 2001). Interestingly, Nxt1 was also reported to interact with Nxf2 (Herold et al., 2001; Herold et al., 2000). Both Nxf2 and Nxt1 were previously identified in screens for piRNA-guided silencing in somatic and germline cells, and their depletion resulted in female sterility (Czech et al., 2013; Handler et al., 2013; Muerdter et al., 2013). Contrary to expectations based upon previous findings (Sienski et al., 2015; Yu et al., 2015), we saw no enrichment for Piwi by mass spectrometry (Figure 1A), results that are consistent with another recent study (Batki et al., 2019). However, co-immunoprecipitation experiments detected weak but reproducible interactions between Piwi and Panx, Nxf2, and Nxt1, but not with a negative control (Figure 1—figure supplement 1D), suggesting that low amounts of transposon substrates in unperturbed cells and/or transient associations might push Piwi below the limit of detection by less sensitive approaches.

Using CRISPR/Cas9, we generated flies that express a GFP-Nxf2 fusion protein from the endogenous *nxf2* locus. GFP-Nxf2 is expressed in follicle and germline cells of the ovary and localizes predominantly to nuclei (Figure 1C and Figure 1—figure supplement 1C). Mass spectrometry of GFP-Nxf2-associated proteins identified Panx, Nxf2, and Nxt1, as binding partners (Figure 1D, Figure 1-Source Data 2), implying the existence of a complex containing these three factors, which we named the Panx-induced co-transcriptional silencing (PICTS) complex.

We therefore generated two nxf2 mutant alleles, $nxf2^{F10*}$ and $nxf2^{\Delta 1*}$, which harbor premature stop codons that disrupt the *nxf2* open reading frame from amino acid 10 onwards (Figure 1B and Figure 1—figure supplement 1E). Trans-heterozygous mutants were female sterile, with fewer eggs laid and none hatching (Figure 1—figure supplement 1F). *nxf2* mutants were severely

compromised in the repression of soma- and germline-specific transposons, in a highly similar manner to *panx* mutants (Figure 1E), with no change in piRNA levels or Piwi localization, despite compromised silencing (Figure 1—figure supplement 1G-H).

To assess the specificity of the impact of *nxf2* mutations on the transcriptome, we performed RNA-seq from total RNA of heterozygote and mutant ovaries, using *panx* mutants for comparison. As reported previously, the expression of protein-coding genes was not generally affected in *nxf2* mutants, with only 16 out of 7,252 (r^2=0.963) being changed more than 4-fold (Figure 1F) (Herold et al., 2001; Herold et al., 2003). In contrast, 28 out of 60 transposon families (that were above the expression threshold of 1 rpm) were de-repressed by more than 4-fold in *nxf2* mutants. Similar results were obtained for *panx* mutants: 16 out of 60 transposons were de-repressed and only 6 out of 7,252 genes mis-regulated (r^2=0.991). ChIP-seq for the H3K9me3 mark from *nxf2* mutant ovaries showed reduced methylation levels at the same transposon families that were de-repressed according to RNA-seq, such as *Het-A*, while randomly chosen genomic intervals were not changed (Figure 1—figure supplement 2A-B).

Ovarian somatic cells (OSCs), cultured *in vitro*, express a functional piRNA-guided co-transcriptional gene silencing machinery and provide a convenient context for mechanistic studies (Saito et al., 2009). RNA-seq from OSCs depleted of Piwi, Panx or Nxf2 showed marked de-repression of soma-specific (e.g. *mdg1, gypsy*, *297*) and intermediate transposon families (e.g. *blood*) when compared to control cells treated with *GFP* siRNAs (Figure 1G left; Figure 1—figure supplement 2C). The de-repression of transposon families strongly correlates with the reduction in H3K9me3 levels mapped over their consensus sequences in ChIP-seq samples generated from the same knockdowns (Figure 1G right). In contrast, no major changes in H3K9me3 were detected over transposons that show no de-repression in these cells upon *piwi*, *panx,* or *nxf2* knockdown.

We next focused on a set of 233 individual, Piwi-regulated genomic transposon insertions in OSCs (see methods for details). This enabled analysis of chromatin states on individual loci, including flanking regions, rather than averaging contributions over a consensus sequence (Figure 1—figure supplement 2D-H). Piwi depletion resulted in the accumulation of H3K4me2 at these loci and spreading of the mark, indicative of active transcription, beyond the transposon into downstream regions (Figure 1—figure supplement 2D, F), similar to earlier reports (Donertas et al., 2013; Klenov et al., 2014; Sienski et al., 2012). Knockdown of *panx* or *nxf2* showed similar, though less pronounced, effects. H3K9me3 marks were strongly reduced upon Piwi depletion, with *panx* and *nxf2* knockdowns showing a similar but milder impact (Figure 1—figure supplement 2E,G). H3K4me2 spreading typically correlates with increased RNA output and a decrease in H3K9me3 levels, as evident for a euchromatic *gypsy* insertion located within an intron of the 5' UTR of the gene *ex* on chromosome 2L (Figure 1—figure supplement 2H).

Panx and Nxf2 proteins are interdependent for their stability

Proteins that form complexes are often interdependent for either localization or stability, and there are abundant examples of such interactions in the piRNA pathway (Donertas et al., 2013; Ohtani et al., 2013). To test for such dependencies among TGS factors, we depleted Piwi, Panx or Nxf2 in germ cells of flies expressing GFP-Nxf2 (Figure 2A) or GFP-Panx (Figure 2B). Germline knockdown of *piwi* had no effect on the localization of either Nxf2 or Panx. Depletion of Panx, however, led to a pronounced loss of nuclear GFP-Nxf2 in nurse cell nuclei (Figure 2A). The reciprocal was also true, with GFP-Panx nuclear signal being reduced upon *nxf2* knockdown in nurse cells (Figure 2B). Similarly, the individual depletion of Panx or Nxf2 in follicle cells resulted in a reduction of both proteins (Figure 2—figure supplement 1A-B). To assess whether the observed reduction reflects protein stability rather than mislocalization, we performed western blots on ovarian lysates. Panx protein level was strongly reduced in *nxf2* mutant ovaries (Figure 2C) and GFP-Nxf2 signal was completely lost in homozygous *panx* mutants (Figure 2D). Of note, mRNA levels of Nxf2 and Panx were not affected when the other factor was mutated (Figure 1F), implying regulation at the protein level. Considered together, the localization and stability of Nxf2 and Panx are interdependent *in vivo*.

PICTS complex formation is required for TGS

To map the domains of Nxf2 and Panx that mediate their interaction, we expressed various combinations of full-length, truncated, or mutant proteins in S2 cells or in OSCs where native protein expression had been reduced by RNAi (Figure 3A). Interactions were tested by co-immunoprecipitation and western blot analyses, and the subcellular localization analyzed by immunofluorescence staining. In OSCs, the ability of each construct to rescue transposon de-repression was monitored by qPCR.

Full-length Nxf2 and Panx robustly co-immunoprecipitated (Figure 3B) and co-localized in S2 cell nuclei (Figure 3C). Removing the carboxy-terminal half of Panx (Panx-ΔC) yielded a protein that remained nuclear, while co-expressed Nxf2 remained largely cytoplasmic, and these proteins no longer formed a complex (Figure 3B-D). When expressed alone in S2 cells, Nxf2 remained predominantly cytoplasmic (ZsGreen-HA in Figure 3C), suggesting that interaction with Panx is necessary for nuclear localization of Nxf2. Panx-ΔN, in contrast, retained the ability to interact with Nxf2 but failed to localize to the nucleus (Figure 3B-D). Strikingly, enforced localization of Panx-ΔN to the nucleus also restored nuclear localization of Nxf2 (Figure 3D and Figure 3—figure supplement 1C-D). Deleting only either the coiled coil domain #2 or C-terminal region, which together make up most of the carboxy-terminal half of Panx, reduced co-purification with Nxf2 (Figure 3D and Figure 3—figure supplement 1C), with neither construct being able to rescue *mdg1* repression upon *panx* knockdown (Figure 3E). Overall, these results suggest that the N-terminal part of Panx carries its nuclear localization signal that aids proper localization of Nxf2 via interaction with the Panx C-terminal region.

To probe the regions of Nxf2 that are essential for its function, we expressed, in the presence of full-length Panx, Nxf2 proteins that lacked either the regions required for RNA cargo binding or the region essential for its association with the NPC (Braun et al., 2001; Fribourg et al., 2001; Herold et al., 2001) (Figure 3A and Figure 3—figure supplement 2A left). Nxf2-ΔNPC failed to co-purify with Panx, and this was accompanied by an increased cytoplasmic protein localization (Figure 3B-D). In contrast, deleting the cargo-binding region of Nxf2 had less impact on its co-purification with Panx or the nuclear localization of either protein (Figure 3B-D). This mutant was able to interact with Panx-ΔN but not Panx-ΔC, as expected (Figure 3F). Mutants of Nxf2, which had individual domains removed, uniformly failed to rescue *nxf2* knockdown in OSCs (Figure 3—figure supplement 2D), yet all but Nxf2-ΔUBA still co-purified with full-length Panx (Figure 3D and Figure 3—figure supplement 2B-C). We also generated point mutants within the UBA domain, altering 2-4 highly conserved amino acids at a time (Figure 3—figure supplement 2A right). UBA mutant #1, showed a phenotype similar to the domain deletion with reduced binding to Panx, increased cytoplasmic localization, and failure to rescue loss of Nxf2 (Figure 3B-E and Figure 3—figure supplement 2E-F). Thus, the interaction of Nxf2 and Panx relies on an intact UBA domain and requires the carboxy-terminal portion of Panx.

The NTF2-like fold was previously shown to mediate the interaction of NXF proteins with Nxt1 (Herold et al., 2000; Kerkow et al., 2012; Suyama et al., 2000). To probe a potential requirement for Nxt1 in silencing, we generated NTF2 domain point mutants in residues involved in the interaction with Nxt1 (Kerkow et al., 2012). All four Nxf2-NTF2 point mutants localized predominantly to the nucleus and co-precipitated quantities of Panx comparable to the full-length control (Figure 3D and Figure 3—figure supplement 2E-F). Yet, three mutants (#1, #2, and #3) failed to rescue transposon de-repression upon depletion of Nxf2 (Figure 3E), pointing to an involvement of Nxt1 in silencing. Indeed, reduced amounts of Nxt1 were recovered with the NTF2 mutants #1 and #2, while the NTF2 mutant #4, which rescued transposon expression (Figure 3E), as well as UBA mutants #1 and #2 showed levels comparable to full-length Nxf2 (Figure 3G and Figure 3—figure supplement 2G).

Tethering of Nxf2 and Nxt1 to RNA triggers silencing

Artificial tethering of Panx to nascent RNA or DNA was previously shown to result in co-transcriptional silencing and the concurrent accumulation of repressive chromatin marks (Sienski et al., 2015; Yu et al., 2015). To test whether Nxf2 could induce TGS, we created an integrated sensor comprising the *Drosophila simulans* ubiquitin promoter driving an HA-tagged ZsGreen transcript with 9 BoxB sites in its 3' UTR in OSCs (Figure 4A). As expected from previous studies (Sienski et al., 2015; Yu et al., 2015), expression of λN-Piwi did not lead to reduced RNA or protein levels (Figure 4B and Figure 4—figure supplement 1A), although it did localize to nuclei (Figure 4—figure supplement 1B). Tethering of λN-Panx, in contrast, resulted in robust repression of sensor RNA and protein signals, as reported (Sienski et al., 2015; Yu et al., 2015). λN-Nxf2 caused an even stronger reduction of RNA

and protein expression from the reporter (Figure 4B). FISH experiments supported consistent repression by Panx and Nxf2 (Figure 4—figure supplement 1C). Tethering of λN-Nxt1 also induced reporter repression (Figure 4B). Strikingly, upon tethering of Nxt1, Nxf2 or Panx, we observed increased levels of H3K9me3 over the reporter (Figure 4C). These data suggest that Nxf2 and Nxt1, along with Panx, act as key effectors of co-transcriptional silencing and are each sufficient to recruit the downstream silencing machinery.

We also tested whether Nxf2 could silence artificial targets upon tethering to DNA rather than nascent transcripts. Our sensor construct carried 8 LacO sites upstream of the *D. sim.* ubiquitin promoter, which drives the expression of HA-ZsGreen (Figure 4D). While tethering of LacI-Piwi did not affect sensor expression, LacI-Panx resulted in robust reductions in both RNA and protein levels (Figure 4E and Figure 4—figure supplement 1D), as previously reported (Sienski et al., 2015). LacI-Nxf2 also silenced the reporter, reducing both mRNA and protein output, albeit to a lesser extent than LacI-Panx tethering. Surprisingly, LacI-Nxt1 was unable to silence the sensor construct. Repression by tethered Panx or Nxf2 resulted in a striking decrease in H3K4me2 marks over the transcribed parts (i.e. promoter and ZsGreen coding region), while the remainder of the reporter showed low read coverage and little difference in the prevalence of the mark (Figure 4—figure supplement 1E). Conversely, H3K9me3 increased upon repression (Figure 4F). Of note, the entire reporter sequence (except a small gap around the LacO site and the 3' UTR where the mappability is poor) was prominently decorated with H3K9me3, suggesting spreading of this chromatin mark following initial silencing.

The data presented above identified functional elements within Nxf2 and Panx that are required for proper localization, interaction, and Piwi-dependent transcriptional gene silencing. We next examined the ability of Panx and Nxf2 mutants to silence our artificial DNA reporters, thus bypassing Piwi-piRNA dependent target recognition. Neither LacI-Nxf2-ΔCargo nor LacI-Panx-ΔN, which were predicted to interact with their full-length partner in OSCs (Figure 3B-D), were able to repress the sensor (Figure 4G). Yet, LacI-Panx-ΔC, which could not interact with Nxf2, substantially reduced RNA and protein expression from the sensor, with its effects as robust as upon DNA tethering of LacI-HP1a (Figure 4G). This suggests that the amino-terminal part of Panx is necessary and sufficient to enforce silencing of an artificial reporter independent of its interaction with Nxf2.

Discussion

Our data identify Nxf2 and Nxt1 as critical mediators of co-transcriptional gene silencing, acting in concert with Panx to repress loci in response to Piwi-piRNA target engagement (Figure 4H). The emerging model for piRNA-dependent silencing implies that target recognition by Piwi is necessary to recruit the PICTS complex onto the appropriate nascent RNA targets. Difficulties in detecting stable interactions between Piwi and PICTS components *in vivo* may arise from a requirement for Piwi target engagement to licence it for recruitment of silencing complexes, as has been suggested previously (Sienski et al., 2015; Yu et al., 2015). The same mechanism may underlie the difficulties experienced in observing Piwi on its target loci by ChIP (Marinov et al., 2015).

We find that Panx and Nxf2 are interdependent for their protein stability and proper subcellular localization, underscoring the fact that correct assembly of the PICTS complex is essential for TGS, while the silencing capacity, per se, resides in Panx. Of note, previous work reported a partial destabilization of Nxf2 in cells depleted of Nxt1 (Herold et al., 2001), potentially extending the interdependency to all three proteins. RIP-seq experiments from unperturbed cells found transposon RNAs enriched only with Panx, as reported (Sienski et al., 2015), but not with Nxf2 (Figure 4—figure supplement 1F), possibly due to low substrate availability combined with an insensitive assay. These results are consistent with another recent report that did not detect transposon enrichment in Nxf2 CLIP-seq from wild-type cells (Batki et al., 2019). However, two other studies identified transposon mRNA association with Nxf2 in CLIP-seq experiments upon depletion of the previously described TGS factor, Mael (Zhao et al., 2019), or by using a stable cell line and depletion of endogenous Nxf2 (Murano et al., 2019). Considered together, these data suggest that Nxf2 might be important for stabilizing the binding of Panx to nascent RNAs. However, precisely how Nxf2 executes this function remains to be fully elucidated. Of note, Murano and colleagues find that Panx interacts with Nxf2, Piwi, Mael and Arx (Murano et al., 2019), which could imply that other TGS factors come into contact with the PICTS complex, although the relationship between these factors and PICTS requires further investigation.

Mutational analyses suggest that Panx and Nxf2 must normally bind Nxt1 to carry out transposon repression. Direct recruitment of any of the PICTS complex components to RNA reporters results in robust chromatin silencing. Upon tethering to DNA, however, Panx induces potent TGS, whereas Nxf2 leads to less prominent effects and Nxt1 shows no silencing capability in our assays. Interestingly, recruitment of the amino-terminal part of Panx alone is necessary and sufficient to induce reporter repression, pinpointing this domain of Panx as harboring the silencing effector function. Future investigations will be crucial to uncover the molecular mechanism by which the Panx amino terminus instructs the downstream chromatin silencing machinery.

Our work, and that of others (Batki et al., 2019; Murano et al., 2019; Zhao et al., 2019) indicates that piRNA-guided co-transcriptional silencing of transposons has coopted several components of the RNA export machinery,

namely Nxf2 and Nxt1. Of the four NXF proteins present in flies, only two have thus far been characterized. Interestingly, while Nxf1, acting along with Nxt1, is crucial for canonical mRNA export (Braun et al., 2001; Fribourg et al., 2001; Herold et al., 2001; Wilkie et al., 2001), Nxf2 has been coopted by the piRNA pathway and functions in co-transcriptional gene silencing. Nxf3, which also is required for transposon repression in germ cells (Czech et al., 2013), is emerging as being critical for the export of piRNA precursors generated from dual-strand clusters in the germline (ElMaghraby et al., 2019; Kneuss, E., Munafò, M., Eastwood, E.L., Deumer, U.-S., Preall, J.B., Hannon, G.J., and Czech, B. Specialization of the *Drosophila* nuclear export family protein, Nxf3, for piRNA precursor export. *Submitted to Genes & Development*). The role of Nxf4, whose expression is testis-specific, is yet to be established. This remarkable functional diversity of NXF family members correlates with tissue-specific expression patterns, and seems conserved in mammals (Yang et al., 2001). However, deciphering how each achieves substrate specificity will be critical to understanding how these homologs can be exclusively dedicated to different targets and confer different fates upon the RNAs that they bind.

Importantly, the fate of the nascent transcript that is detected by Piwi and instructed by PICTS for silencing remains unclear. One hypothesis is that instead of being exported, these targets undergo degradation by the nuclear exosome. Such mechanism would be contrary to yeast, where the TREX complex subunit Mlo3 was shown to oppose siRNA-mediated heterochromatin formation at gene loci (Yu et al., 2018), and suggests that different lineages have evolved different silencing mechanisms. In any case, it is possible that a single transcript from a locus that is marked for silencing might pose a lesser threat than an unsilenced locus and, therefore, not be capable of exerting evolutionary pressure for the detemination of its fate.

Materials and Methods

Fly stocks and handling

All flies were kept at 25 °C. Flies carrying a BAC transgene expressing GFP-Panx were generated by the Brennecke lab (Handler et al., 2013). Panx frameshift mutants $panx^{M1}$ and $panx^{M4}$ were described earlier (Yu et al., 2015). The GFP-Nxf2 fusion knock-in and nxf2 frameshift mutations (*nxf2[F10*]* and *nxf2[Δ1*]*) were generated for this study (see below). Control w^{1118} flies were a gift from the University of Cambridge Department of Genetics Fly Facility. For knockdowns we used a stock containing the Dcr2 transgene and a nos-GAL4 driver (described in (Czech et al., 2013)) and dsRNA lines from the VDRC ($panx^{KK102702}$, $nxf2^{KK101676}$, $piwi^{KK101658}$). Fertility of the *nxf2* and *panx* mutant females was scored by crossing ten freshly hatched females to five w^{1118} males and counting the number of eggs laid in 12 hr periods and pupae that developed after 7 days.

Generation of mutant and transgenic fly strains

Frameshift mutant alleles of *nxf2* were generated by injecting pCFD4 (addgene plasmid # 49411; (Port et al., 2014)) containing two gRNAs against Nxf2 (generated by Gibson assembly) into embryos expressing vas-Cas9 (Bloomington stock 51323). To generate GFP-Nxf2 fusion knock-in flies, homology arms of approximately 1 kb were cloned into pUC19 by Gibson assembly and co-injected with pCFD3 (addgene plasmid # 49410; (Port et al., 2014)) containing a single guide RNA into embryos expressing vas-Cas9 (# 51323, Bloomington stock center). Microinjection and fly stock generation was carried out by the University of Cambridge Department of Genetics Fly Facility. Mutant and knock-in flies were identified by genotyping PCRs and confirmed by sanger sequencing.

Immunoprecipitation from ovary lysates and Mass Spectrometry

Ovaries from ~170 GFP-Panx, GFP-Nxf2 and control flies (3-5 days old) were dissected in ice-cold PBS and lysed in 300 µl of CoIP Lysis Buffer (20 mM Tris-HCl pH 7.5, 150 mM NaCl, 2 mM MgCl2, 10% glycerol, 1 mM DTT, 0.1 mM PMSF, 0.2% NP-40 supplemented with complete protease inhibitors [Roche]) and homogenized using a motorized pestle. Lysates were cleared for 5 min at 16000g and the residual pellet re-extracted with the same procedure. GFP-tagged proteins were immunoprecipitated by incubation with 30 µl of GFP-Trap magnetic beads (Chromotek) for 3 hrs at 4 °C on a tube rotator. The beads were washed 6x with Lysis Buffer and 2x with 100 mM Ammonium Bicarbonate, before TMT-labelling followed by quantitative Mass Spectrometry. TMT chemical isobaric labelling were performed as described (Papachristou et al., 2018).

Analysis of Mass Spectrometry data

Raw data were processed in Proteome Discoverer 2.1 software (Thermo Fisher Scientific) using the SequestHT search engine. The data were searched against a database derived from FlyBase ("*dmel-all-translation-r6.24"*) at a 1% spectrum level FDR criteria using Percolator (University of Washington). For the SequestHT node the following parameters were included: Precursor mass tolerance 20 ppm and fragment mass tolerance 0.5

Da. Dynamic modifications were oxidation of M (+15.995 Da), deamidation of N, Q (+0.984 Da) and static modifications were TMT6plex at any N-Terminus and K (+229.163 Da). The consensus workflow included S/N calculation for TMT intensities and only unique peptides identified with high confidence (FDR < 0.01) were considered for quantification. Downstream data analysis was performed on R using the qPLEXanalyzer package (https://doi.org/10.5281/zenodo.1237825) as described (Papachristou et al., 2018). Only proteins with more than one unique peptide were considered.

Cell Culture

Drosophila Ovarian Somatic Cells (OSCs) were a gift from Mikiko Siomi and were cultured at 26 °C in Shields and Sang M3 Insect Medium (Sigma Aldrich) supplemented with 0.6 mg/ml Glutathione, 10% FBS, 10 mU/ml insulin and 10% fly extract (purchased from DGRC) as described (Niki et al., 2006; Saito, 2014; Saito et al., 2009). Cell identity was authenticated by whole genome DNA sequencing in-house. Gibco® *Drosophila* Schneider 2 (S2) cells were purchased from Thermo Fisher Scientific (catalog number R69007) and were grown at 26 °C in Schneider's *Drosophila* Media (Gibco) supplemented with 10% heat-inactivated FBS. Cell identity was characterized by Thermo Fisher Scientific through isozyme and karyotype analysis (see product description). OSCs and S2 cells tested negative for mycoplasma contamination in-house. Knockdowns (all siRNA sequences are given in Supplementary file 1) and transfections in OSCs were carried out as previously described (Saito, 2014). In short, for knockdown experiments $10x10^6$ cells were nucleofected with 200 pmol annealed siRNAs using the Amaxa Cell Line Nucleofector Kit V (Lonza, program T-029). After 48 hrs, $10x10^6$ cells were nucleofected again with 200 pmol of the same siRNA and allowed to grow for an additional 48 hrs before further processing. For rescue experiments, 5 µg of rescue construct plasmid were added to the second knockdown solution. OSCs were transfected with 10 µg of plasmid using Xfect (Clontech), according to manufacturer's instruction. S2 cells were transfected with 2 µg of plasmid using Effectene (Qiagen), according to manufacturer's instructions.

Co-immunoprecipitation from cell lysates

S2 cells or OSCs were transfected with 3xFLAG- and HA-tagged constructs (wild-type and mutants). Cells were harvested 48 hrs after transfection and lysed in 250 µl of CoIP Lysis Buffer (Pierce) supplemented with Complete protease inhibitors (Roche). 200 µg of proteins for each sample were diluted to 1 ml with CoIP Lysis Buffer and the 3xFLAG-tagged bait was immunoprecipitated by incubation with 20 µl of anti-FLAG M2 Magnetic Beads (Sigma M8823) for 2 hrs at 4 °C on a tube rotator. The beads were washed 3x 15 min with TBS supplemented with protease inhibitors. Beads were then resuspended in 2x NuPAGE LDS Sample Buffer (Thermo Fisher Scientific) without reducing agent and boiled for 3 min at 90 °C to elute immunoprecipitated proteins. IPs, unbound fractions and input fractions were diluted to 1x NuPAGE LDS Sample Buffer concentration and reducing agent was added. Samples were boiled at 90 °C for 10 min before separating proteins as described below.

Western Blot

Protein concentration was measured using a Direct Detect Infrared Spectrometer (Merck). 20 µg of proteins were separated on a NuPAGE 4-12% Bis-Tris gel (Thermo Fisher Scientific). Proteins were transferred with an iBLot2 device (Invitrogen) on a nitrocellulose membrane and blocked for 1 hr in 1x Licor TBS Blocking Buffer (Licor). Primary antibodies were incubated over night at 4 °C. Licor secondary antibodies were incubated for 45 min at room temperature (RT) and images acquired with an Odyssey CLx scanner (Licor). The following antibodies were used: anti-HA (ab9110), anti-FLAG (Sigma #F1804), anti-GFP (ab13970), anti-Piwi (described in (Brennecke et al., 2007)), anti-Nxt1 (Herold et al., 2001), anti-Histone H3 (ab10799), anti-Tubulin (ab18251), mouse anti-Panx (Sienski et al., 2015), IRDye® 680RD Donkey anti-Rabbit IgG (H + L) (Licor), IRDye® 800CW Donkey anti-Mouse IgG (H + L) (Licor), IRDye® 800CW Goat anti-Rat IgG (H + L) (Licor).

Immunofluorescence in ovaries

Fly ovaries were dissected in ice-cold PBS and fixed in 4% paraformaldehyde (PFA) at RT for 15 min. After 2 quick rinses in PBS with Triton at 0.3% (PBS-Tr), samples were permeabilized with 3x 10 min washes with PBS-Tr. Samples were then blocked in PBS-Tr with 1% BSA for 2 hrs at RT and then incubated overnight at 4 °C with primary antibodies in PBS-Tr and 1% BSA. The next day, samples were washed 3x 10 min at RT in PBS-Tr and incubated overnight at 4 °C with secondary antibodies in PBS-Tr and 1% BSA. The next day, samples were washed 4x 10 min in PBS-Tr at RT and DAPI (Thermo Fisher Scientific #D1306) was added during the third wash. After 2x 5 min washes in PBS, samples were mounted on slides with ProLong Diamond Antifade Mountant (Thermo Fisher Scientific #P36961) and imaged on a Leica SP8 confocal microscope (63x and 100x Oil objective). The following antibodies were used: chicken anti-GFP (ab13970), rabbit anti-Piwi (described in (Brennecke et al., 2007)), mouse anti-Aub (Senti et al., 2015), anti-Rabbit-555 (Thermo Fisher), anti-Mouse-647 (Thermo Fisher), anti-Chicken-647 (Abcam).

Immunofluorescence from cells

Cells were plated one day in advance on Fibronectin- or Concanavalin A-coated coverslips (for OSCs and S2 cells, respectively), fixed for 15 min in 4% PFA, permeabilized for 10 min in PBS with 0.2% Triton (PBST) and blocked for 30 min in PBS, 0.1% Tween-20 and 1% BSA. Primary antibodies were diluted in PBS, 0.1% Tween-20 and 0.1% BSA and incubated overnight at 4 °C. After 3x 5 min washes in PBST, secondary antibodies were incubated for 1 hr at RT. After 3x 5 min washes in PBST, DAPI was incubated for 10 min at RT, washed 2 times and the coverslips were mounted using ProLong Diamond Antifade Mountant (Thermo Fisher Scientific #P36961) and imaged on a Leica SP8 confocal microscope (100x Oil objective). The following antibodies were used: anti-Lamin (Developmental Studies Hybridoma Bank ADL67.10), anti-HA (ab9111), anti-FLAG (Cell Signaling Technology 14793S), anti-chicken-488 (Abcam), anti-Rabbit-555 (Thermo Fisher), anti-Mouse-647 (Thermo Fisher).

RNA Fluorescent in situ hybridization (RNA FISH)

RNA FISH was performed with Hybridization Chain Reaction (HCR), similar as reported (Ang and Yung, 2016; Choi et al., 2014). OSCs were fixed for 15 min in 4% PFA, washed 2x 5 min with PBS and permeabilized for at least 24 hrs in 70% ethanol at -20 °C. Ethanol was removed and slides washed twice for 5 min in 2x Saline-Sodium Citrate buffer (SSC). Priming for hybridization was done by incubating for 10 min in 15% formamide in 2x SSC. HCR probes were diluted to 1 nM each in hybridization buffer (15% formamide, 10% dextran sulfate in 2x SSC) and incubated overnight at 37 °C in a humidified chamber. Excess probes were removed by rinsing twice in 2x SSC and washing once in 30% formamide for 10 min at 37 °C. HCR hairpins conjugated to AlexaFluor-647® (IDT) were heat-denatured and diluted to 120 nM in 5x SSC and 0.1% Tween-20. HCR amplification was carried out for 2 hrs at RT in the dark and washed 3x 10 min with 5x SSC and 0.1% Tween-20. Nuclei were stained with DAPI for 10 min, followed by 3x 10 min washes in 5x SSC. Slides were mounted with ProLong Diamond Antifade Mountant (Thermo Fisher Scientific) and imaged on a Leica SP8 confocal microscope (100x Oil objective). The sequences of all probes are given in Supplementary file 1.

Image analysis

Intensity plot profiles across individual egg chambers were acquired in Fiji (lines displayed). Intensity values for each channel were averaged over 10 pixels and adjusted as a percentage of the highest value along the profile. A threshold of 30% DAPI intensity was set to define nuclei. Individual egg chambers used for analysis are displayed for each channel with inverted LUT.

Tethering experiments

For RNA tethering, OSCs with a stable integration of the sensor plasmid (pDsimUbi-HA-ZsGreen-NLuc-9xBoxB) were generated in the lab. $4x10^6$ cells were nucleofected with 5 µg of plasmid expressing λN-3xFLAG-tagged constructs, as described above. After 48 hrs, $4x10^6$ cells were nucleofected again with 5 µg of the same plasmid and allowed to grow for an additional 48 hrs before the relative expression of the sensor was analyzed. For DNA tethering, OSCs were transiently transfected with 8xLacO-pDsimUbi-HA-ZsGreen sensor plasmid and LacI-3xFLAG fusion constructs. Cells were allowed to grow for 72 hrs before the relative expression of the sensor was determined.

ChIP-seq from ovaries

Ovaries from 120 to 150 adult flies were dissected in ice-cold PBS, collected in 1.5 ml Bioruptor® Microtubes (Diagenode #C30010016), and immediately frozen at -80 °C. Samples were crosslinked in 1 ml A1 buffer (60 mM KCl, 15 mM NaCl, 15 mM HEPES pH 7.6, 4 mM MgCl2, 0.5% Triton X-100, 0.5 mM dithiothreitol (DTT), 10 mM sodium butyrate and complete EDTA-free protease inhibitor cocktail [Roche #04693159001]), in the presence of 1.8% formaldehyde. Samples were homogenized with a micropestle for 2 min and incubated for a total time of 15 min at RT on a rotating wheel. Crosslinking was stopped by adding 225 mM glycine followed by incubation for 5 min on a

rotating wheel. The homogenate was centrifuged for 5 min at 4,000g at 4 °C. The supernatant was discarded, and the nuclear pellet was washed twice in 1 ml A1 buffer and once in 1 ml of A2 buffer (140 mM NaCl, 15 mM HEPES pH 7.6, 1 mM EDTA, 0.5 mM EGTA, 1% Triton X-100, 0.5 mM DTT, 0.1% sodium deoxycholate, 10 mM sodium butyrate and complete mini EDTA-free protease inhibitor cocktail) at 4 °C. Nuclei were then resuspended in 100 µl A2 buffer with 1% SDS and 0.5% N-laurosylsarcosine and incubated for 2 hrs at 4 °C with agitation at 1,500 rpm. Chromatin was sonicated using a Bioruptor® Pico (Diagenode #B01060010) for 16 cycles of 30 sec on/30 sec off. Sheared chromatin size peaked at 150 bp. After sonication and 5 min high-speed centrifugation at 4 °C, fragmented chromatin was recovered in the supernatant and the final volume was raised to 1 ml in A2 buffer with 0.1% SDS. 50 µl of the diluted samples were used as DNA input control, in a final volume of 200 µl of A2 buffer with 0.1% SDS. Chromatin for IP was precleared by addition of 15 µl of Protein A/G Magnetic Beads (Thermo Fisher Scientific) suspension followed by overnight incubation at 4 °C. Beads were removed by centrifugation, and anti-H3K9me3 (Active Motif #39161) antibody was added (1:200 dilution) to 5 µg of chromatin and incubated for 4 hrs at 4 °C on a rotating wheel. 50 µl of Protein A/G Magnetic Beads were added, and incubation was continued overnight at 4 °C. Antibody-protein complexes were washed 4 times in A3 (A2+ 0.05% SDS) buffer and twice in 1 mM EDTA, 10 mM Tris (pH 8) buffer for 5 minutes at 4 °C on a rotating wheel. Chromatin was eluted from the beads in 200 µl of 10 mM EDTA, 1% SDS, 50 mM Tris (pH 8) for 30 min with agitation at 1,500 rpm and then reverse-crosslinked overnight at 65 °C, together with the input DNA. IP and input samples were treated with 2 µl of Proteinase K (Thermo Fisher Scientific #EO0491) for 3 hrs at 56 °C. DNA was purified using the MinElute PCR purification Kit (Thermo Fisher Scientific), according to manufacturer's instructions, and resuspended in 30 µl water. Recovered DNA was quantified with Qubit 4 Fluorometer (Thermo Fisher Scientific) and analysed with Agilent Bioanalyzer 2100 High Sensitivity DNA Chip (Agilent). DNA libraries were prepared with NEBNext® Ultra™ II DNA Library Prep Kit for Illumina® (NEB), according to manufacturer's instructions. DNA libraries were quantified with KAPA Library Quantification Kit for Illumina (Kapa Biosystems) and deep-sequenced with Illumina HiSeq 4000 (Illumina).

ChIP-seq from OSCs

For ChIP from OSCs we adapted a protocol by Schmidt and colleagues(Schmidt et al., 2009). In short, $10x10^6$ OSCs were crosslinked in 1% formaldehyde for 10 min. Crosslinking was quenched by addition of glycine solution, followed by 3 washes in ice-cold PBS. Crosslinked cells were either snap-frozen in liquid nitrogen and stored at -80 °C or processed immediately. Cells were resuspended in 1 ml buffer LB1 (50 mM HEPES-KOH pH 7.5, 140 mM NaCl, 1 mM EDTA, 10% glycerol, 0.5% Igepal CA-630, 0.25% Triton-X 100, EDTA-free protease inhibitor cocktail [Roche]) and incubated on ice for 10 min while inverting several times. Cells were centrifuged for 5 min at 2,000g at 4 °C. Supernatant was discarded and pellet resuspended in 1 ml LB2 10 mM Tris-HCL pH 8.0, 200 mM NaCl, 1 mM EDTA, 0.5 M EGTA, EDTA-free protease inhibitor cocktail). Cells were incubated on ice for 5 min and centrifuged again. Isolated nuclei were

resuspended in 300 µl sonication buffer LB3 (10 mM Tris-HCL pH 8, 100 mM NaCl, 1 mM EDTA, 0.5 mM EGTA, 0.1% Na-Deoxycholate, 0.5% N-lauroylsarcosine, EDTA-free protease inhibitor cocktail) and transferred in 1.5 ml Bioruptor® Microtubes (Diagenode). Chromatin was sonicated using a Bioruptor® Pico (Diagenode) for 16 cycles of 30 sec on/30 sec off. Sheared chromatin size peaked at 150 bp. The lysate was cleared by high-speed centrifugation at 4 °C. 100 µl Protein A Dynabeads (Thermo Fisher Scientific) were incubated with 5 µl H3K9me3 (Active Motif #39161) or H3K4me2 antibody (Millipore # 07-030) over night at 4 °C while rotating. The cleared lysate was split in two equal fractions and a 5 µl input fraction was saved for further processing. Lysate volumes were adjusted to 300 µl with LB3 and Triton-X 100 was added to a final concentration of 1%. Lysates were incubated with either H3K9me3 or H3K4me2 coated beads over night at 4 °C while rotating. Washing, reverse-crosslinking, DNA purification and library preparation was done as described above (ChIP-seq from ovaries).

RNA isolation

Cell pellets or fly ovaries were lysed in 1ml Trizol and RNA was extracted using RNeasy mini prep column (Qiagen), according to manufacturer's instructions.

qPCR analysis

1 µg of total RNA was treated with DNAseI (Thermo Fisher Scientific), according to manufacturer's instructions. Reverse transcription was performed with Superscript III First Strand Synthesis Kit (Thermo Fisher Scientific), using oligo$(dT)_{20}$ primers, according to the manufacturer's instructions. Real-time PCR (qPCR) experiments were performed with a QuantStudio Real-Time PCR Light Cycler (Thermo Fisher Scientific). Transposon levels were quantified using the $\Delta\Delta$CT method (Livak and Schmittgen, 2001), normalized to *rp49* and fold changes were calculated relative to the indicated controls. All oligonucleotide sequences are given in Supplementary file 1.

RIP-seq from ovaries

Ovaries from ~100 GFP-Panx or GFP-Nxf2 flies (3-5 days old) were dissected in ice-cold PBS and fixed with 0.1% PFA for 20 min, followed by quenching with equal volumes of 125 mM Glycine. Fixed ovaries were lysed in 200 µl of RIPA Buffer (supplemented with complete protease inhibitors (Roche) and RNasin Plus 40 U/ml) and homogenized using a motorized pestle. Lysates were incubated 3 min at 37 °C with 4 µl of Turbo DNase, incubated 20 min at 4 °C on a tube rotator and sonicated with a Bioruptor® Pico (3 cycles of 30 sec on/30 sec off). Lysates were pre-cleared using 40 µl of Pierce Protein A/G beads for 1 hr at 4 °C and GFP-tagged proteins were immunoprecipitated by incubation with 50 µl of GFP-Trap magnetic agarose beads (Chromotek) overnight at 4 °C. An aliquot of pre-cleared input lysate was saved for RNA isolation and library preparation. Following 3 washes in 150 mM KCl, 25 mM Tris (pH 7.5), 5 mM EDTA, 0.5% NP40, 0.5 mM DTT (supplemented with protease inhibitors and RNasin Plus 1:1000), IP and input samples were reverse crosslinked in 1x Reverse Crosslinking buffer (PBS, 2% Nlauroyl sarcosine, 10 mM EDTA, 5 mM DTT) and Proteinase K. RNA isolation was performed using Trizol and 100 ng of input or IP RNA were used for library

preparation using the SMARTer stranded RNA-seq Kit (Clontech). DNA libraries were quantified with KAPA Library Quantification Kit for Illumina (Kapa Biosystems) and deep-sequenced with Illumina HiSeq 4000 (Illumina).

Small RNA-seq library preparation

Small RNA libraries were generated as described previously(Jayaprakash et al., 2011). Briefly, 18- to 29-nt-long small RNAs were purified by PAGE from 10 µg of total ovarian RNA. Next, the 3' adapter (containing four random nucleotides at the 5' end) was ligated overnight using T4 RNA ligase 2, truncated KQ (NEB). Following recovery of the products by PAGE purification, the 5' adapter (containing four random nucleotides at the 3' end) was ligated to the small RNAs using T4 RNA ligase (Abcam) for 1 hr. Small RNAs containing both adapters were recovered by PAGE purification, reverse transcribed and PCR amplified prior quantification using the Library Quantification Kit for Illumina (Kapa Biosystems) and sequenced on an Illumina HiSeq 4000 (Illumina). All adapter sequences are given in Supplementary file 1.

RNA-seq library preparation

1 µg of total RNA was used as input material for library preparation. The NEBNext Poly(A) mRNA magnetic Isolation Module (NEB) was used to isolate poly(A) RNAs. Libraries were generated with the NEBNext Ultra Directional RNA Library Prep kit for Illumina (NEB) according to manufacturer's instructions. The pooled libraries were quantified with KAPA Library Quantification Kit for Illumina (Kapa Biosystems) and sequenced on an Illumina HiSeq 4000 (Illumina).

RNA-seq, small RNA-seq, RIP-seq and ChIP-seq analysis

Raw fastq files generated by Illumina sequencing were analysed by a pipeline developed in-house. In short, the first and last base of each 50 bp read were removed using fastx trimmer (http://hannonlab.cshl.edu/fastx_toolkit/). RIP-seq reads were first aligned against rRNAs and mapped reads discarded. High-quality reads were aligned to the *Drosophila melanogaster* genome release 6 (dm6) downloaded from Flybase using STAR (Dobin et al., 2013). For transposon-wide analysis, genome multi-mapping reads were randomly assigned to one location using option '--outFilterMultimapNmax 1000 --outMultimapperOrder Random' and non-mapping reads were removed. Alignment files were then converted back to fastq format with samtools (Li et al., 2009) and re-aligned to the transposon consensus sequences allowing multi-mappers that were assigned to a random position. Generated bam alignment files were indexed using samtools index. For genome-wide analyses, multi-mapping reads were removed to ensure unique locations of reads. Normalization was achieved by calculating rpm (reads per million) using the deepTools2 bamCoverage function (Ramirez et al., 2016) with 10 bp bin sizes. The scaling factor for transposon mapping reads was calculated from reads that aligned to transposon consensus sequences relative to genome aligned reads. Reads mapping to genes were counted with htseq (Anders et al., 2015) and transposon derived reads were calculated using a custom script (available with this article as Source Code File 1). Metaplots flanking euchromatic insertion sites and transposon coverage plots were

calculated by deepTools2 with bin sizes of 10 bp and 50 bp, respectively. Stranded RNA libraries were trimmed, aligned and indexed as described above. Alignment files were split in sense and antisense reads using samtools view. Normalization of the split alignment files as well as feature counting was performed as described above. For transposon expression analysis only sense reads were considered. Differential expression analysis was performed using a custom build R script (available with this article as Source Code File 2). Adapters from raw small RNA fastq files were clipped with fastx_clipper (adapter sequence AGATCGGAAGAGCACACGTCTGAACTCCAGTCA) keeping only reads with at least 23 bp length. Then the first and last 4 bases were trimmed using seqtk (https://github.com/lh3/seqtk). Alignment and normalization were performed as described above. Only high-quality small RNA reads with a length between 23 and 29 bp were used for further analysis of piRNA profiles. piRNA distribution was calculated and plotted in R. For piRNA coverage plots over TEs, only the 5' position of reads was plotted.

Generation of annotation files for RNA-seq and ChIP-seq analysis

The locations of euchromatic transposon insertions in OSCs were derived from Sienski et al., 2012 and updated to dm6 genome release coordinates using the UCSC liftOver tool. Transposon consensus sequences were downloaded from Flybase. Mappability tracks for dm6 with 50 bp resolution were calculated as described (Derrien et al., 2012). Piwi-dependent OSC insertions were defined by comparing H3K9me3 signal intensities of siRNA-mediated knockdowns for *gfp* and *piwi*. Signal was counted by htseq using a customized GTF file including the locations of all euchromatic TE insertions in OSCs and reads were normalized to rpm. TE insertions were annotated as Piwi-dependent if the ratio of normalized signal intensity of GFP knockdown versus Piwi knockdown was higher than 2.

Plotting and data visualization

Random genomic windows for box plots of H3K9me3 ChIP-seq data were calculated using BEDtools' random function (Quinlan and Hall, 2010) with bin size 5,000 bp, bin number 1,000 and random seed number 800. 100 random windows were chosen (number 200-300) and analysed along with ChIP-seq data for de-repressed TEs and those not affected. Welch two sample t-test was applied for statistics. Metaplots of euchromatic TE insertions as well as TE coverage plots for RNA-seq and ChIP-seq data were generated with deepTools2 and Adobe Illustrator. Scatterplots for differentially expressed transposons and genes were generated with R package ggplot2. Heatmaps were calculated with deepTools2 and data plotted in R. For scatterplots, only TEs and genes with a scaled read count larger than 1 (rpm > 1) were used in the analysis and included in plots.

Quantification and Statistical Analysis

Statistical analysis applied to qPCR data sets was calculated by unpaired (two sample) t Test. The number of biological replicates is indicated in the figure legends. Statistical analysis applied to data sets displayed as box plots (Figure 1—figure supplement 2A) was calculated by Welch two sample t-test.

Data Availability

Sequencing data reported in this paper has been deposited in Gene Expression Omnibus under ID code GSE121661. Mass Spectrometry data has been deposited to PRIDE Archive under ID code PXD011415.

Acknowledgements

We thank the CRUK Cambridge Institute Bioinformatics, Genomics, Microscopy and Proteomics Core Facilities for technical support. We thank Aled Perry for his help in establishing a ChIP protocol for OSCs. We thank Karan Metha for help with image analysis. We thank the University of Cambridge Department of Genetics Fly Facility for microinjection services and fly stock generation. We thank the Vienna Drosophila Resource Center and the Bloomington Stock Center for fly stocks, J. Brennecke for anti-Aub and anti-Panx antibodies, and E. Izaurralde for anti-Nxt1 antibody. Research in the Hannon laboratory is supported by Cancer Research UK and by Wellcome Trust award 110161/Z/15/Z. F.C. is supported by an EMBO Long-Term fellowship. M.M. is supported by a Boehringer Ingelheim Fonds PhD fellowship.

Declaration of interests

The authors declare no competing interests.

References

Anders, S., Pyl, P.T., and Huber, W. (2015). HTSeq--a Python framework to work with high-throughput sequencing data. Bioinformatics *31*, 166-169.

Ang, Y.S., and Yung, L.Y. (2016). Rational design of hybridization chain reaction monomers for robust signal amplification. Chem Commun (Camb) *52*, 4219-4222.

Batki, J., Schnabl, J., Wang, J., Handler, D., Andreev, V.I., Stieger, C.E., Novatchkova, M., Lampersberger, L., Kauneckaite, K., Xie, W*., et al.* (2019). The nascent RNA binding complex SFiNX licenses piRNA-guided heterochromatin formation. bioRxiv *doi: https://doi.org/10.1101/609693*.

Braun, I.C., Herold, A., Rode, M., Conti, E., and Izaurralde, E. (2001). Overexpression of TAP/p15 heterodimers bypasses nuclear retention and stimulates nuclear mRNA export. J Biol Chem *276*, 20536-20543.

Brennecke, J., Aravin, A.A., Stark, A., Dus, M., Kellis, M., Sachidanandam, R., and Hannon, G.J. (2007). Discrete small RNA-generating loci as master regulators of transposon activity in Drosophila. Cell *128*, 1089-1103.

Choi, H.M., Beck, V.A., and Pierce, N.A. (2014). Next-generation in situ hybridization chain reaction: higher gain, lower cost, greater durability. ACS Nano *8*, 4284-4294.

Czech, B., Munafo, M., Ciabrelli, F., Eastwood, E.L., Fabry, M.H., Kneuss, E., and Hannon, G.J. (2018). piRNA-Guided Genome Defense: From Biogenesis to Silencing. Annu Rev Genet *52*, 131-157.

Czech, B., Preall, J.B., McGinn, J., and Hannon, G.J. (2013). A transcriptome-wide RNAi screen in the Drosophila ovary reveals factors of the germline piRNA pathway. Mol Cell *50*, 749-761.

Derrien, T., Estelle, J., Marco Sola, S., Knowles, D.G., Raineri, E., Guigo, R., and Ribeca, P. (2012). Fast computation and applications of genome mappability. PLoS One *7*, e30377.

Dobin, A., Davis, C.A., Schlesinger, F., Drenkow, J., Zaleski, C., Jha, S., Batut, P., Chaisson, M., and Gingeras, T.R. (2013). STAR: ultrafast universal RNA-seq aligner. Bioinformatics *29*, 15-21.

Donertas, D., Sienski, G., and Brennecke, J. (2013). Drosophila Gtsf1 is an essential component of the Piwi-mediated transcriptional silencing complex. Genes Dev *27*, 1693-1705.

ElMaghraby, M.F., Andersen, P.R., Pühringer, F., Meixner, K., Lendl, T., Tirian, L., and Brennecke, J. (2019). A heterochromatin-specific RNA export pathway facilitates piRNA production. bioRxiv *doi: https://doi.org/10.1101/596171*.

Fribourg, S., Braun, I.C., Izaurralde, E., and Conti, E. (2001). Structural basis for the recognition of a nucleoporin FG repeat by the NTF2-like domain of the TAP/p15 mRNA nuclear export factor. Mol Cell *8*, 645-656.

Gunawardane, L.S., Saito, K., Nishida, K.M., Miyoshi, K., Kawamura, Y., Nagami, T., Siomi, H., and Siomi, M.C. (2007). A slicer-mediated mechanism for repeat-associated siRNA 5' end formation in Drosophila. Science *315*, 1587-1590.

Handler, D., Meixner, K., Pizka, M., Lauss, K., Schmied, C., Gruber, F.S., and Brennecke, J. (2013). The genetic makeup of the Drosophila piRNA pathway. Mol Cell *50*, 762-777.

Herold, A., Klymenko, T., and Izaurralde, E. (2001). NXF1/p15 heterodimers are essential for mRNA nuclear export in Drosophila. RNA *7*, 1768-1780.

Herold, A., Suyama, M., Rodrigues, J.P., Braun, I.C., Kutay, U., Carmo-Fonseca, M., Bork, P., and Izaurralde, E. (2000). TAP (NXF1) belongs to a multigene family of putative RNA export factors with a conserved modular architecture. Mol Cell Biol *20*, 8996-9008.

Herold, A., Teixeira, L., and Izaurralde, E. (2003). Genome-wide analysis of nuclear mRNA export pathways in Drosophila. EMBO J *22*, 2472-2483.

Iwasaki, Y.W., Murano, K., Ishizu, H., Shibuya, A., Iyoda, Y., Siomi, M.C., Siomi, H., and Saito, K. (2016). Piwi Modulates Chromatin Accessibility by Regulating Multiple Factors Including Histone H1 to Repress Transposons. Mol Cell *63*, 408-419.

Jayaprakash, A.D., Jabado, O., Brown, B.D., and Sachidanandam, R. (2011). Identification and remediation of biases in the activity of RNA ligases in small-RNA deep sequencing. Nucleic Acids Res *39*, e141.

Kerkow, D.E., Carmel, A.B., Menichelli, E., Ambrus, G., Hills, R.D., Jr., Gerace, L., and Williamson, J.R. (2012). The structure of the NXF2/NXT1 heterodimeric complex reveals the combined specificity and versatility of the NTF2-like fold. J Mol Biol *415*, 649-665.

Klenov, M.S., Lavrov, S.A., Korbut, A.P., Stolyarenko, A.D., Yakushev, E.Y., Reuter, M., Pillai, R.S., and Gvozdev, V.A. (2014). Impact of nuclear Piwi elimination on chromatin state in Drosophila melanogaster ovaries. Nucleic Acids Res *42*, 6208-6218.

Klenov, M.S., Sokolova, O.A., Yakushev, E.Y., Stolyarenko, A.D., Mikhaleva, E.A., Lavrov, S.A., and Gvozdev, V.A. (2011). Separation of stem cell maintenance and transposon silencing functions of Piwi protein. Proc Natl Acad Sci U S A *108*, 18760-18765.

Le Thomas, A., Rogers, A.K., Webster, A., Marinov, G.K., Liao, S.E., Perkins, E.M., Hur, J.K., Aravin, A.A., and Toth, K.F. (2013). Piwi induces piRNA-guided transcriptional silencing and establishment of a repressive chromatin state. Genes Dev *27*, 390-399.

Levesque, L., Guzik, B., Guan, T., Coyle, J., Black, B.E., Rekosh, D., Hammarskjold, M.L., and Paschal, B.M. (2001). RNA export mediated by tap involves NXT1-dependent interactions with the nuclear pore complex. J Biol Chem *276*, 44953-44962.

Li, H., Handsaker, B., Wysoker, A., Fennell, T., Ruan, J., Homer, N., Marth, G., Abecasis, G., Durbin, R., and Genome Project Data Processing, S. (2009). The Sequence Alignment/Map format and SAMtools. Bioinformatics *25*, 2078-2079.

Livak, K.J., and Schmittgen, T.D. (2001). Analysis of relative gene expression data using real-time quantitative PCR and the 2(-Delta Delta C(T)) Method. Methods *25*, 402-408.

Marinov, G.K., Wang, J., Handler, D., Wold, B.J., Weng, Z., Hannon, G.J., Aravin, A.A., Zamore, P.D., Brennecke, J., and Toth, K.F. (2015). Pitfalls of mapping high-throughput sequencing data to repetitive sequences: Piwi's genomic targets still not identified. Dev Cell *32*, 765-771.

Muerdter, F., Guzzardo, P.M., Gillis, J., Luo, Y., Yu, Y., Chen, C., Fekete, R., and Hannon, G.J. (2013). A genome-wide RNAi screen draws a genetic framework for transposon control and primary piRNA biogenesis in Drosophila. Mol Cell *50*, 736-748.

Murano, K., Iwasaki, Y.W., Ishizu, H., Mashiko, A., Shibuya, A., Kondo, S., Adachi, S., Suzuki, S., Saito, K., Natsume, T.*, et al.* (2019). Nuclear RNA export factor variant initiates piRNA-guided co-transcriptional silencing. bioRxiv *doi: https://doi.org/10.1101/605725*.

Niki, Y., Yamaguchi, T., and Mahowald, A.P. (2006). Establishment of stable cell lines of Drosophila germ-line stem cells. Proc Natl Acad Sci U S A *103*, 16325-16330.

Ohtani, H., Iwasaki, Y.W., Shibuya, A., Siomi, H., Siomi, M.C., and Saito, K. (2013). DmGTSF1 is necessary for Piwi-piRISC-mediated transcriptional transposon silencing in the Drosophila ovary. Genes Dev *27*, 1656-1661.

Ozata, D.M., Gainetdinov, I., Zoch, A., O'Carroll, D., and Zamore, P.D. (2019). PIWI-interacting RNAs: small RNAs with big functions. Nat Rev Genet *20*, 89-108.

Papachristou, E.K., Kishore, K., Holding, A.N., Harvey, K., Roumeliotis, T.I., Chilamakuri, C.S.R., Omarjee, S., Chia, K.M., Swarbrick, A., Lim, E.*, et al.* (2018). A quantitative mass spectrometry-based approach to monitor the dynamics of endogenous chromatin-associated protein complexes. Nat Commun *9*, 2311.

Port, F., Chen, H.M., Lee, T., and Bullock, S.L. (2014). Optimized CRISPR/Cas tools for efficient germline and somatic genome engineering in Drosophila. Proc Natl Acad Sci U S A *111*, E2967-2976.

Quinlan, A.R., and Hall, I.M. (2010). BEDTools: a flexible suite of utilities for comparing genomic features. Bioinformatics *26*, 841-842.

Ramirez, F., Ryan, D.P., Gruning, B., Bhardwaj, V., Kilpert, F., Richter, A.S., Heyne, S., Dundar, F., and Manke, T. (2016). deepTools2: a next generation web server for deep-sequencing data analysis. Nucleic Acids Res *44*, W160-165.

Rangan, P., Malone, C.D., Navarro, C., Newbold, S.P., Hayes, P.S., Sachidanandam, R., Hannon, G.J., and Lehmann, R. (2011). piRNA production requires heterochromatin formation in Drosophila. Curr Biol *21*, 1373-1379.

Rozhkov, N.V., Hammell, M., and Hannon, G.J. (2013). Multiple roles for Piwi in silencing Drosophila transposons. Genes Dev *27*, 400-412.

Saito, K. (2014). RNAi and overexpression of genes in ovarian somatic cells. Methods Mol Biol *1093*, 25-33.

Saito, K., Inagaki, S., Mituyama, T., Kawamura, Y., Ono, Y., Sakota, E., Kotani, H., Asai, K., Siomi, H., and Siomi, M.C. (2009). A regulatory circuit for piwi by the large Maf gene traffic jam in Drosophila. Nature *461*, 1296-1299.

Schmidt, D., Wilson, M.D., Spyrou, C., Brown, G.D., Hadfield, J., and Odom, D.T. (2009). ChIP-seq: using high-throughput sequencing to discover protein-DNA interactions. Methods *48*, 240-248.

Senti, K.A., Jurczak, D., Sachidanandam, R., and Brennecke, J. (2015). piRNA-guided slicing of transposon transcripts enforces their transcriptional silencing via specifying the nuclear piRNA repertoire. Genes Dev *29*, 1747-1762.
Sienski, G., Batki, J., Senti, K.A., Donertas, D., Tirian, L., Meixner, K., and Brennecke, J. (2015). Silencio/CG9754 connects the Piwi-piRNA complex to the cellular heterochromatin machinery. Genes Dev *29*, 2258-2271.
Sienski, G., Donertas, D., and Brennecke, J. (2012). Transcriptional silencing of transposons by Piwi and maelstrom and its impact on chromatin state and gene expression. Cell *151*, 964-980.
Suyama, M., Doerks, T., Braun, I.C., Sattler, M., Izaurralde, E., and Bork, P. (2000). Prediction of structural domains of TAP reveals details of its interaction with p15 and nucleoporins. EMBO Rep *1*, 53-58.
Wang, S.H., and Elgin, S.C. (2011). Drosophila Piwi functions downstream of piRNA production mediating a chromatin-based transposon silencing mechanism in female germ line. Proc Natl Acad Sci U S A *108*, 21164-21169.
Wilkie, G.S., Zimyanin, V., Kirby, R., Korey, C., Francis-Lang, H., Van Vactor, D., and Davis, I. (2001). Small bristles, the Drosophila ortholog of NXF-1, is essential for mRNA export throughout development. RNA *7*, 1781-1792.
Yang, J., Bogerd, H.P., Wang, P.J., Page, D.C., and Cullen, B.R. (2001). Two closely related human nuclear export factors utilize entirely distinct export pathways. Mol Cell *8*, 397-406.
Yu, R., Wang, X., and Moazed, D. (2018). Epigenetic inheritance mediated by coupling of RNAi and histone H3K9 methylation. Nature *558*, 615-619.
Yu, Y., Gu, J., Jin, Y., Luo, Y., Preall, J.B., Ma, J., Czech, B., and Hannon, G.J. (2015). Panoramix enforces piRNA-dependent cotranscriptional silencing. Science *350*, 339-342.
Zhao, K., Cheng, S., Miao, N., Xu, P., Lu, X., Zhang, Y., Wang, M., Ouyang, X., Yuan, X., Liu, W*., et al.* (2019). A Pandas complex adapted for piRNA-guided transposon silencing. bioRxiv *doi: https://doi.org/10.1101/608273*.

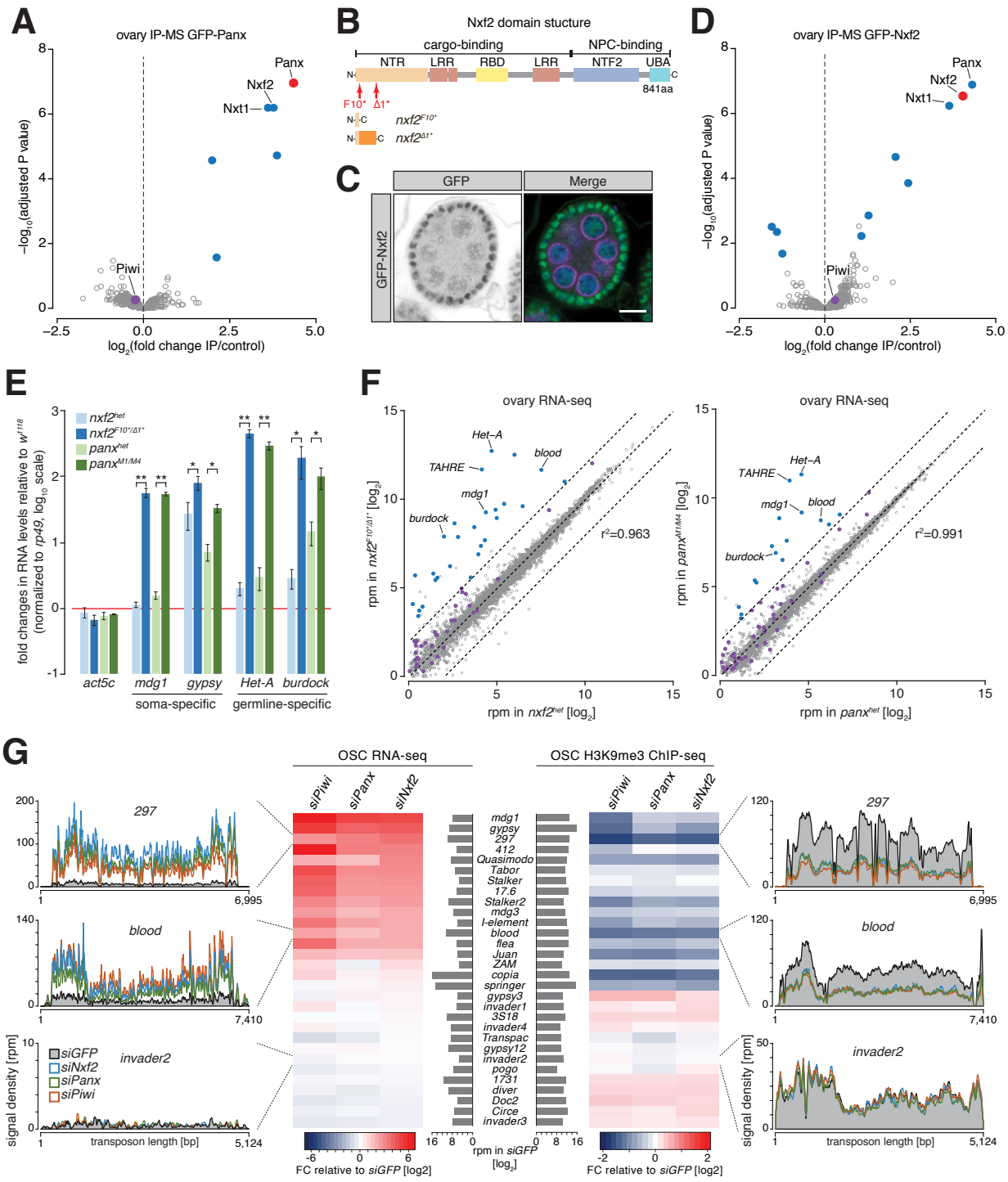
A
ovary IP-MS GFP-Panx
Panx
Nxf2
Nxt1
Piwi
−log10(adjusted P value)
log2(fold change IP/control)
B
Nxf2 domain stucture
cargo-binding
NPC-binding
NTR
LRR
RBD
LRR
NTF2
UBA
841aa
F10*
Δ1*
nxf2F10*
nxf2Δ1*
C
GFP
Merge
GFP-Nxf2
D
ovary IP-MS GFP-Nxf2
E
fold changes in RNA levels relative to w1118 (normalized to rp49, log10 scale)
nxf2het
nxf2F10*/Δ1*
panxhet
panxM1/M4
act5c
mdg1
gypsy
Het-A
burdock
soma-specific
germline-specific
F
ovary RNA-seq
Het–A
TAHRE
blood
mdg1
burdock
r2=0.963
r2=0.991
rpm in nxf2het [log2]
rpm in panxhet [log2]
G
OSC RNA-seq
OSC H3K9me3 ChIP-seq
siPiwi
siPanx
siNxf2
297
blood
invader2
siGFP
siNxf2
siPanx
siPiwi
transposon length [bp]
FC relative to siGFP [log2]
rpm in siGFP [log2]
mdg1
gypsy
297
412
Quasimodo
Tabor
Stalker
17.6
Stalker2
mdg3
I-element
blood
flea
Juan
ZAM
copia
springer
gypsy3
invader1
3S18
invader4
Transpac
gypsy12
invader2
pogo
1731
diver
Doc2
Circe
invader3

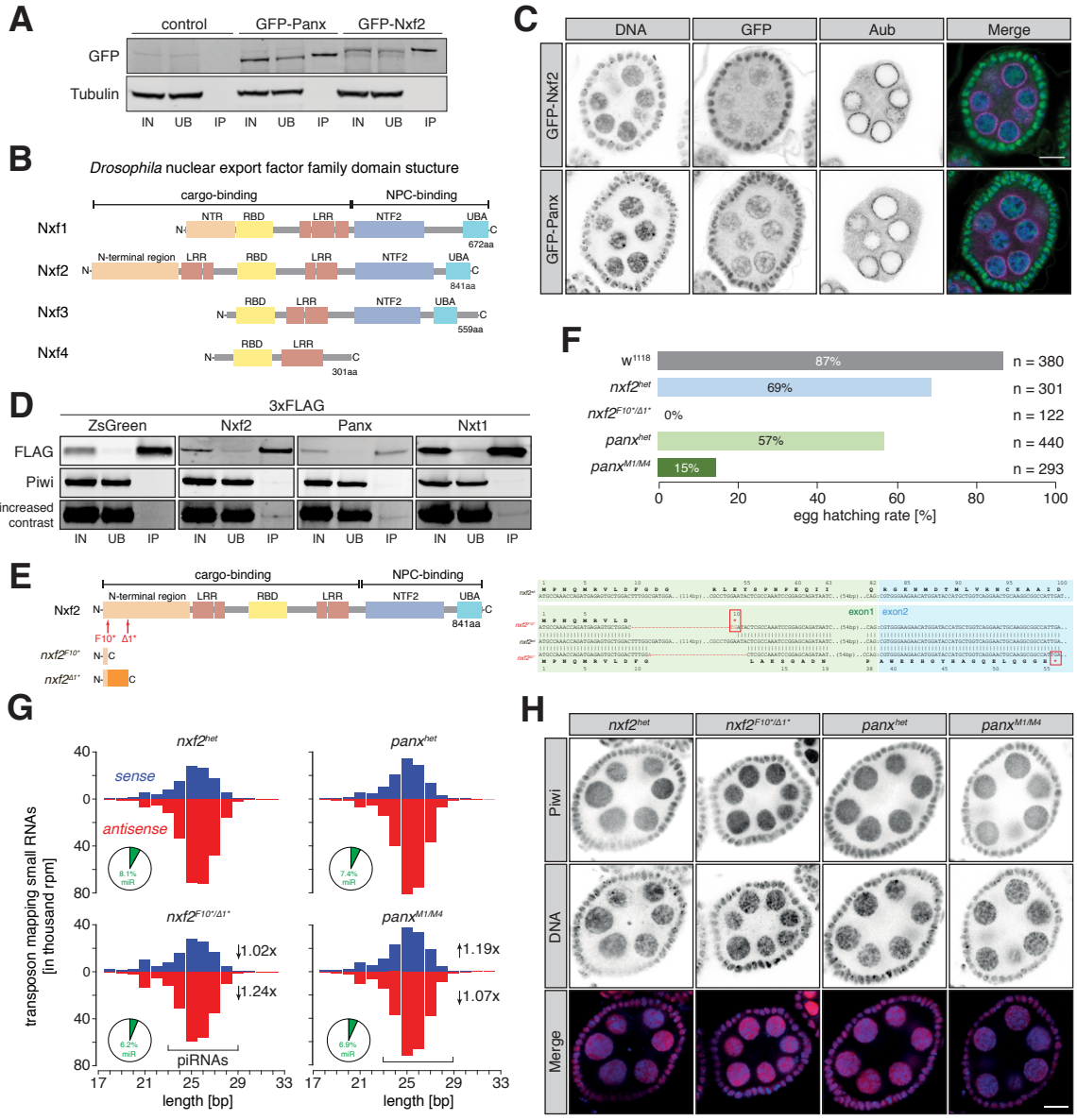
A
control
GFP-Panx
GFP-Nxf2
GFP
Tubulin
IN UB IP IN UB IP IN UB IP
B
Drosophila nuclear export factor family domain stucture
cargo-binding
NPC-binding
Nxf1
NTR RBD LRR NTF2 UBA
672aa
Nxf2
N-terminal region LRR RBD LRR NTF2 UBA
841aa
Nxf3
RBD LRR NTF2 UBA
559aa
Nxf4
RBD LRR
301aa
C
DNA
GFP
Aub
Merge
GFP-Nxf2
GFP-Panx
D
3xFLAG
ZsGreen
Nxf2
Panx
Nxt1
FLAG
Piwi
increased contrast
IN UB IP IN UB IP IN UB IP IN UB IP
E
cargo-binding
NPC-binding
Nxf2
N-terminal region LRR RBD LRR NTF2 UBA
841aa
F10* Δ1*
nxf2F10*
nxf2Δ1*
exon1
exon2
F
w1118
nxf2het
nxf2F10*/Δ1*
panxhet
panxM1/M4
87%
69%
0%
57%
15%
n = 380
n = 301
n = 122
n = 440
n = 293
0 20 40 60 80 100
egg hatching rate [%]
G
nxf2het
panxhet
sense
antisense
nxf2F10*/Δ1*
panxM1/M4
↓1.02x
↓1.24x
↑1.19x
↓1.07x
piRNAs
transposon mapping small RNAs [in thousand rpm]
length [bp]
H
nxf2het
nxf2F10*/Δ1*
panxhet
panxM1/M4
Piwi
DNA
Merge

Fabry, Ciabrelli, Munafò et al., Figure 1—figure supplement 2

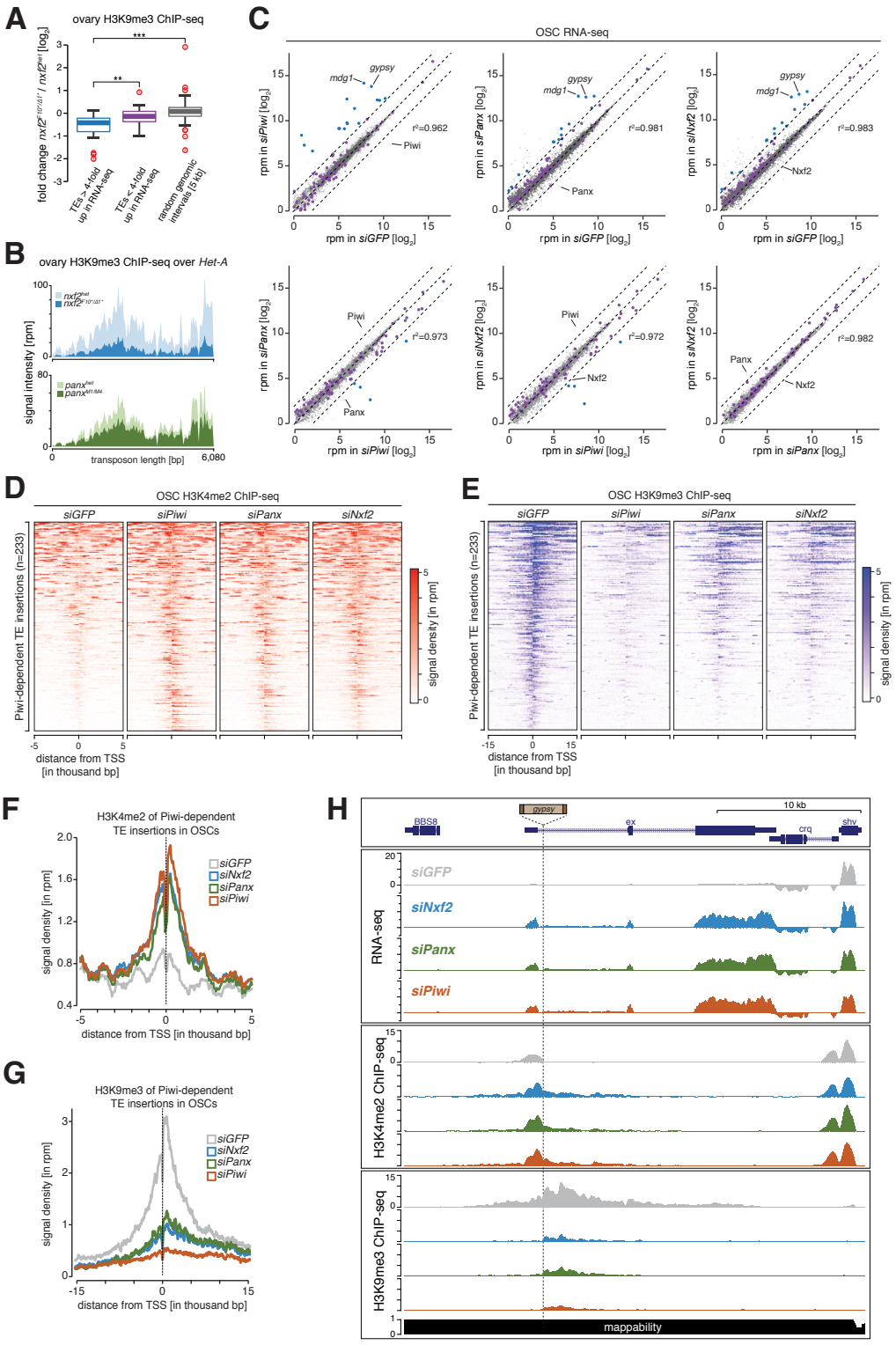

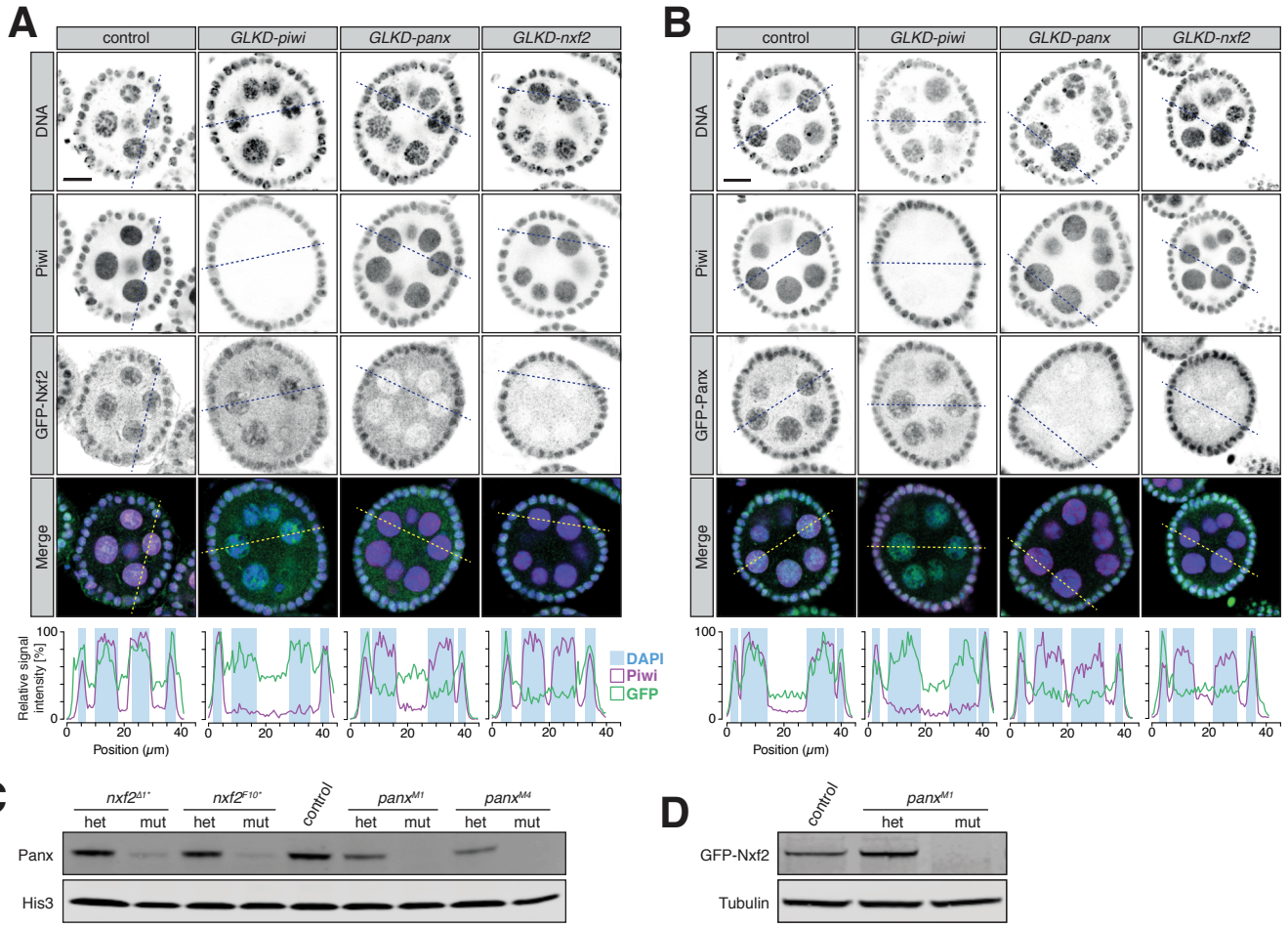
A
control
GLKD-piwi
GLKD-panx
GLKD-nxf2
DNA
Piwi
GFP-Nxf2
Merge
Relative signal intensity [%]
100
0
0
20
40
Position (μm)
DAPI
Piwi
GFP
B
control
GLKD-piwi
GLKD-panx
GLKD-nxf2
DNA
Piwi
GFP-Panx
Merge
Position (μm)
C
nxf2Δ1*
nxf2F10*
control
panxM1
panxM4
het
mut
Panx
His3
D
control
panxM1
het
mut
GFP-Nxf2
Tubulin

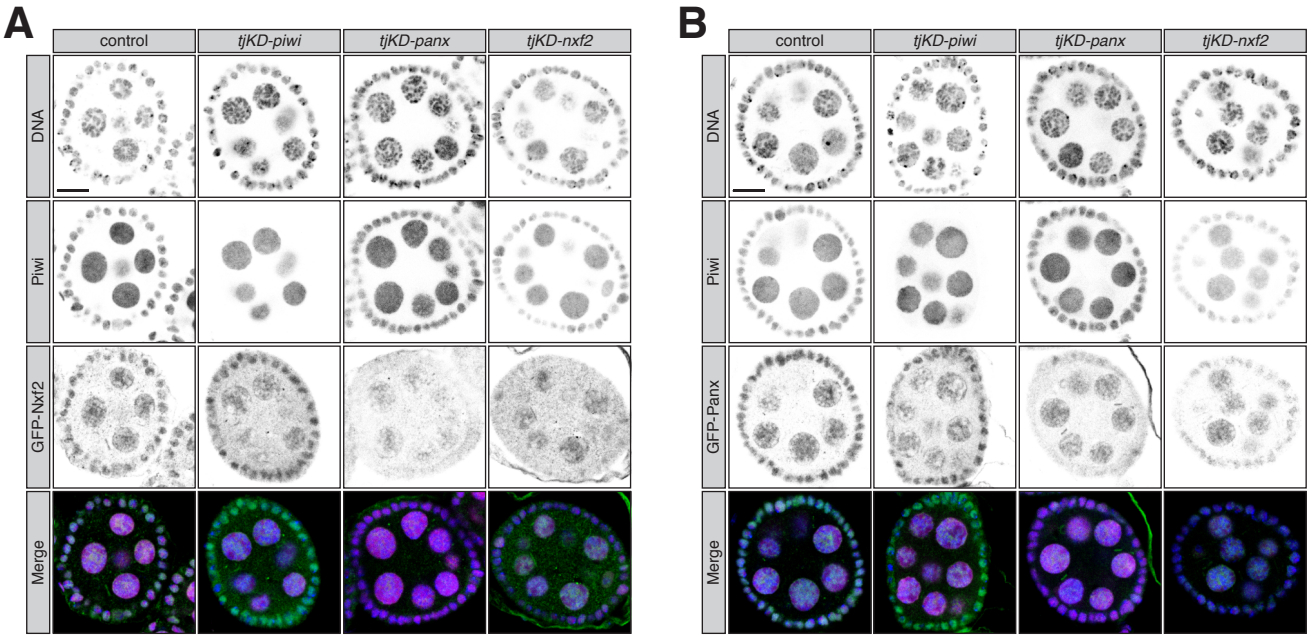
A
control
tjKD-piwi
tjKD-panx
tjKD-nxf2
DNA
Piwi
GFP-Nxf2
Merge
B
control
tjKD-piwi
tjKD-panx
tjKD-nxf2
DNA
Piwi
GFP-Panx
Merge

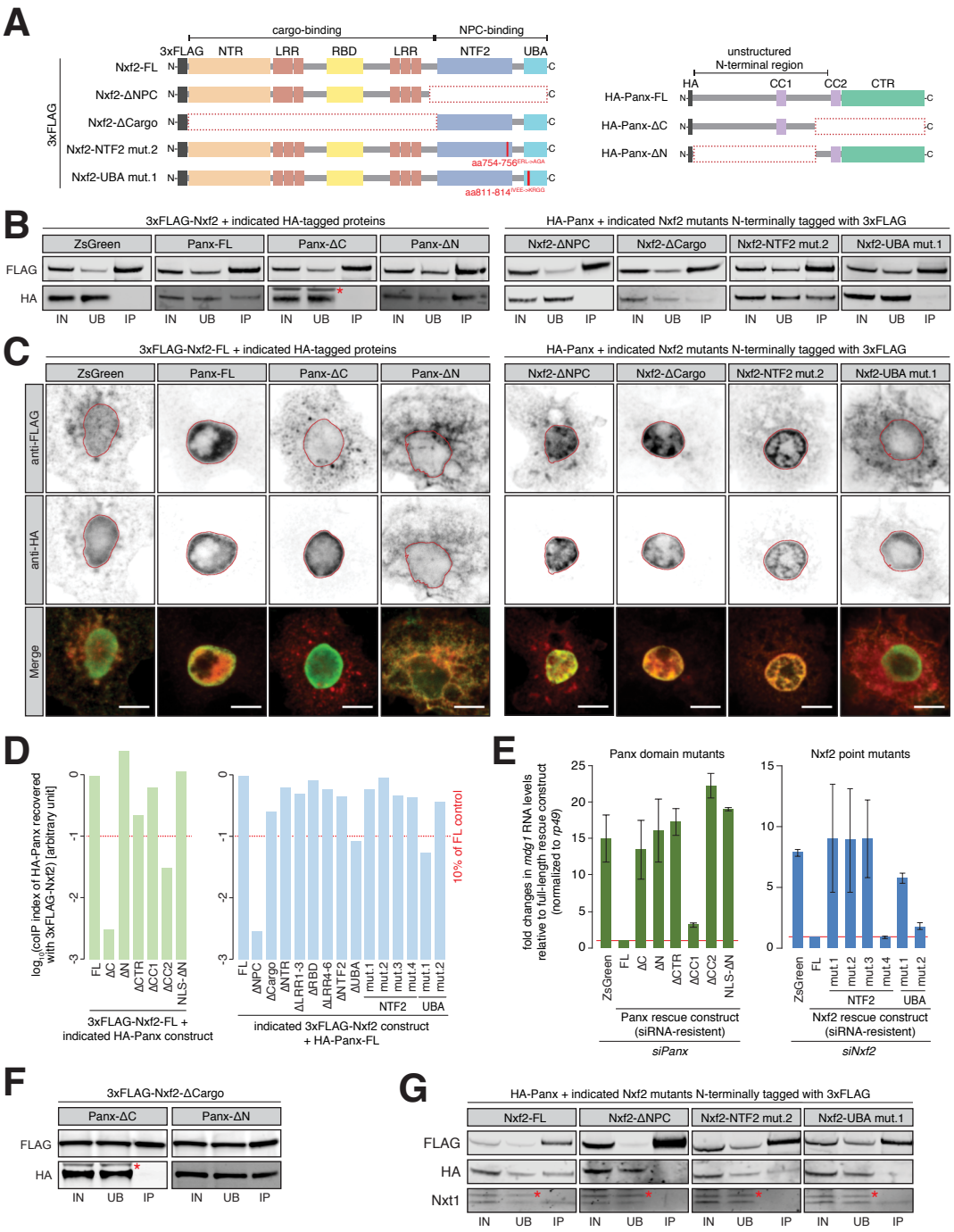
A
cargo-binding
NPC-binding
3xFLAG
NTR
LRR
RBD
LRR
NTF2
UBA
Nxf2-FL
Nxf2-ΔNPC
Nxf2-ΔCargo
Nxf2-NTF2 mut.2
aa754-756ERL>AGA
Nxf2-UBA mut.1
aa811-814WEE>ARGG
unstructured
N-terminal region
HA
CC1
CC2
CTR
HA-Panx-FL
HA-Panx-ΔC
HA-Panx-ΔN
B
3xFLAG-Nxf2 + indicated HA-tagged proteins
HA-Panx + indicated Nxf2 mutants N-terminally tagged with 3xFLAG
ZsGreen
Panx-FL
Panx-ΔC
Panx-ΔN
Nxf2-ΔNPC
Nxf2-ΔCargo
Nxf2-NTF2 mut.2
Nxf2-UBA mut.1
FLAG
HA
IN UB IP
C
3xFLAG-Nxf2-FL + indicated HA-tagged proteins
HA-Panx + indicated Nxf2 mutants N-terminally tagged with 3xFLAG
anti-FLAG
anti-HA
Merge
D
log10(coIP index of HA-Panx recovered with 3xFLAG-Nxf2) [arbitrary unit]
10% of FL control
FL
ΔC
ΔN
ΔCTR
ΔCC1
ΔCC2
NLS-ΔN
3xFLAG-Nxf2-FL + indicated HA-Panx construct
ΔNPC
ΔCargo
ΔNTR
ΔLRR1-3
ΔRBD
ΔLRR4-6
ΔNTF2
ΔUBA
mut.1
mut.2
mut.3
mut.4
NTF2
UBA
indicated 3xFLAG-Nxf2 construct + HA-Panx-FL
E
fold changes in mdg1 RNA levels relative to full-length rescue construct (normalized to rp49)
Panx domain mutants
Nxf2 point mutants
ZsGreen
Panx rescue construct (siRNA-resistent)
siPanx
Nxf2 rescue construct (siRNA-resistent)
siNxf2
F
3xFLAG-Nxf2-ΔCargo
G
HA-Panx + indicated Nxf2 mutants N-terminally tagged with 3xFLAG
Nxt1

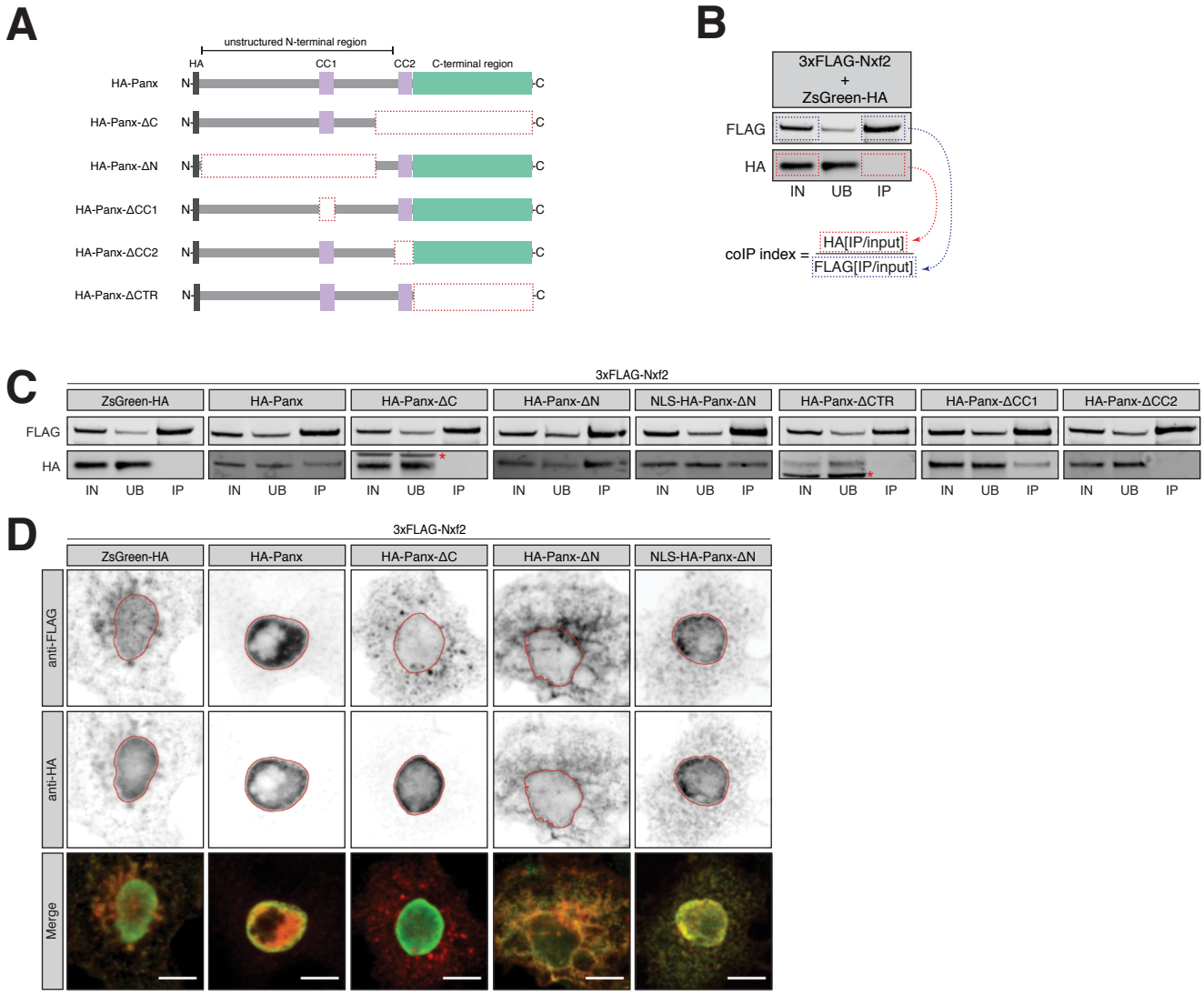
A
unstructured N-terminal region
HA
CC1
CC2
C-terminal region
HA-Panx
HA-Panx-ΔC
HA-Panx-ΔN
HA-Panx-ΔCC1
HA-Panx-ΔCC2
HA-Panx-ΔCTR
N
C
B
3xFLAG-Nxf2
+
ZsGreen-HA
FLAG
HA
IN
UB
IP
coIP index =
HA[IP/input]
FLAG[IP/input]
C
3xFLAG-Nxf2
ZsGreen-HA
HA-Panx
HA-Panx-ΔC
HA-Panx-ΔN
NLS-HA-Panx-ΔN
HA-Panx-ΔCTR
HA-Panx-ΔCC1
HA-Panx-ΔCC2
FLAG
HA
IN
UB
IP
D
3xFLAG-Nxf2
ZsGreen-HA
HA-Panx
HA-Panx-ΔC
HA-Panx-ΔN
NLS-HA-Panx-ΔN
anti-FLAG
anti-HA
Merge

Fabry, Ciabrelli, Munafò et al., Figure 3—figure supplement 2

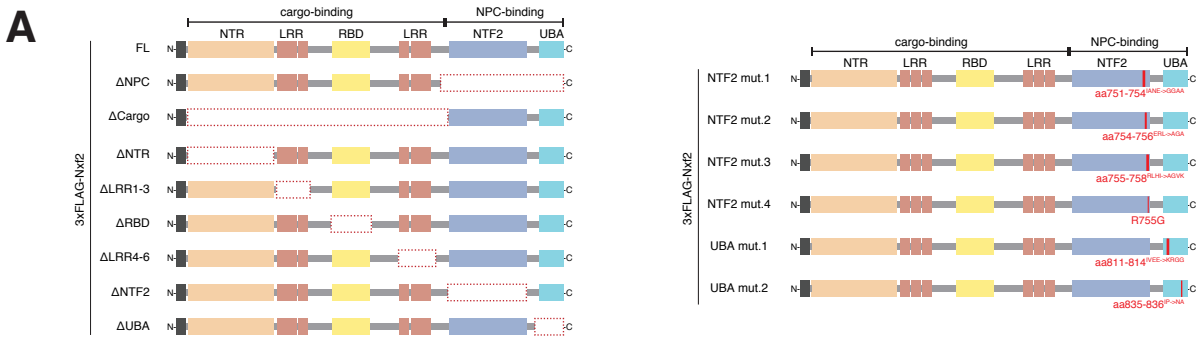

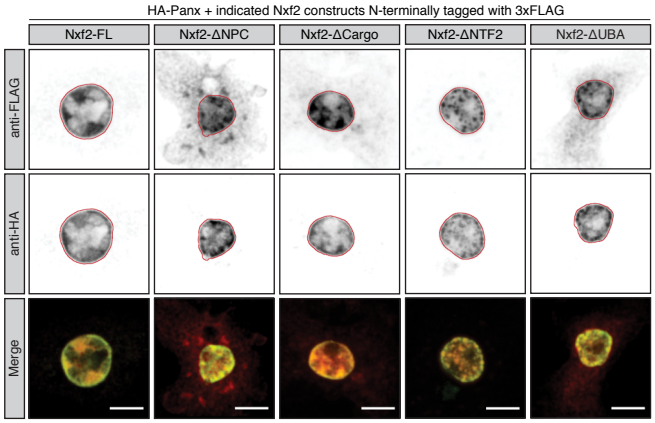

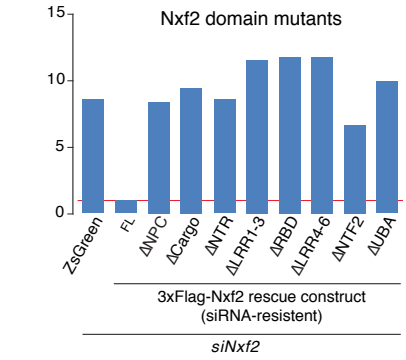

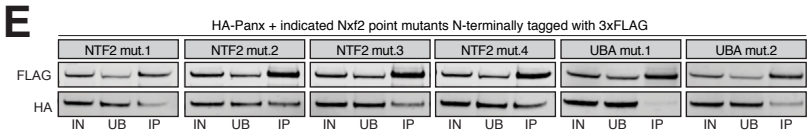

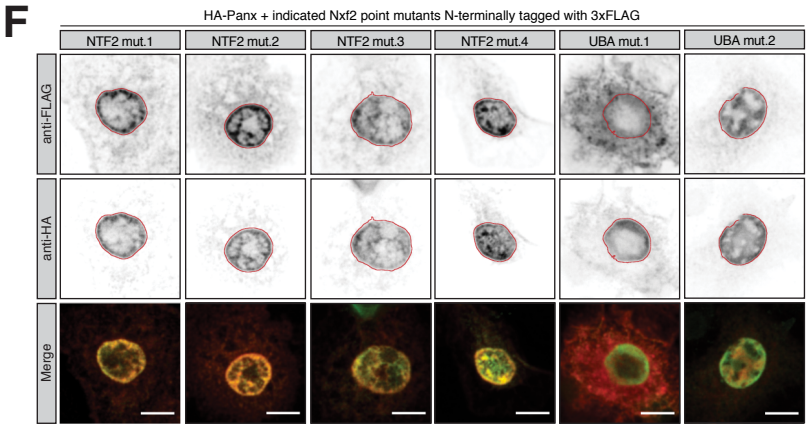

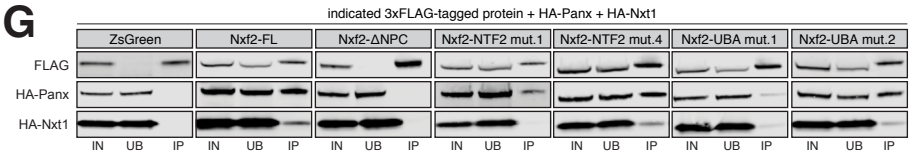

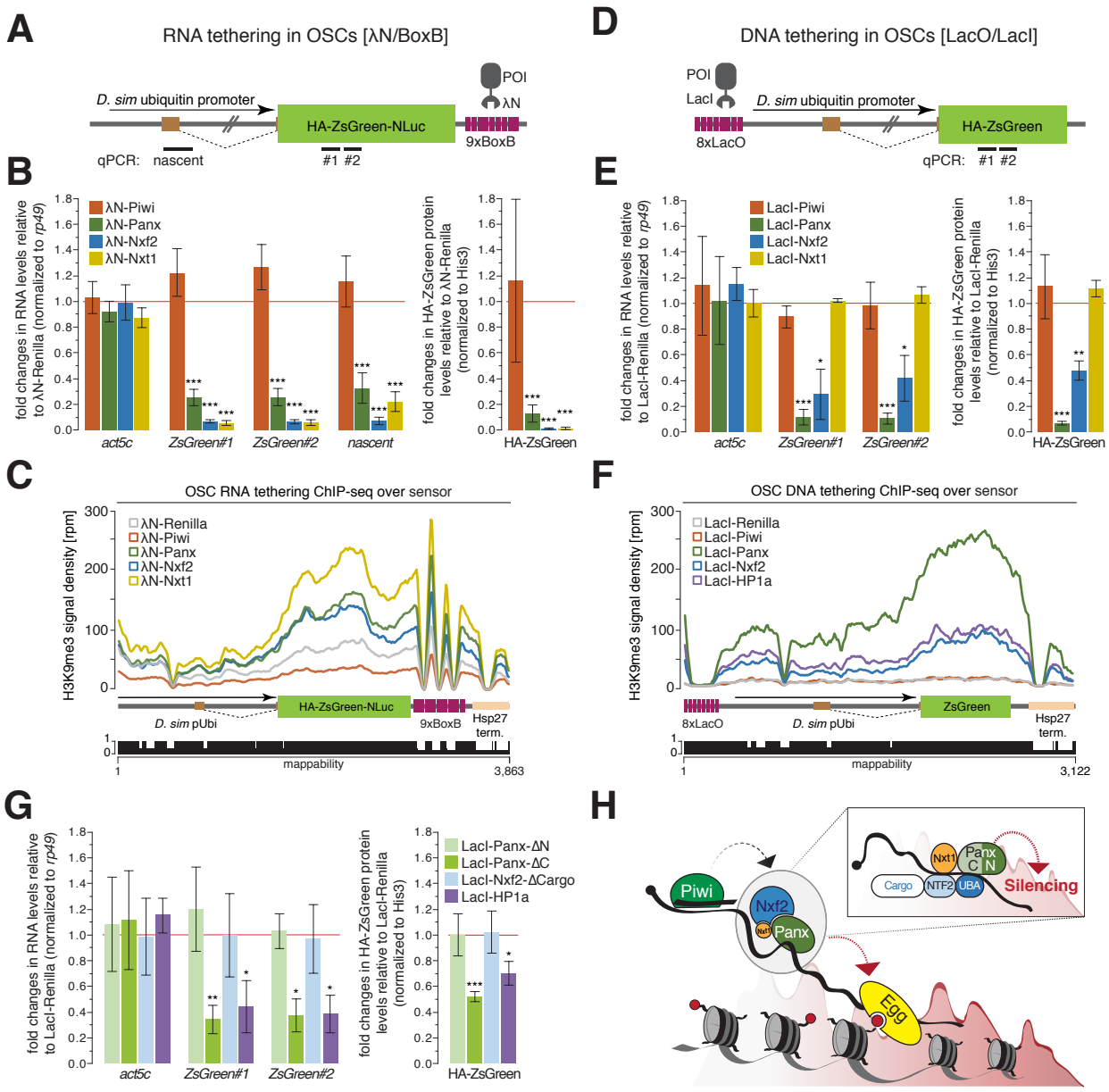
A
RNA tethering in OSCs [λN/BoxB]
D. sim ubiquitin promoter
HA-ZsGreen-NLuc
POI
λN
9xBoxB
qPCR: nascent
#1 #2
B
λN-Piwi
λN-Panx
λN-Nxf2
λN-Nxt1
fold changes in RNA levels relative to λN-Renilla (normalized to rp49)
fold changes in HA-ZsGreen protein levels relative to λN-Renilla (normalized to His3)
act5c
ZsGreen#1
ZsGreen#2
nascent
HA-ZsGreen
C
OSC RNA tethering ChIP-seq over sensor
H3K9me3 signal density [rpm]
λN-Renilla
λN-Piwi
λN-Panx
λN-Nxf2
λN-Nxt1
HA-ZsGreen-NLuc
D. sim pUbi
9xBoxB
Hsp27 term.
mappability
1
3,863
D
DNA tethering in OSCs [LacO/LacI]
POI
LacI
D. sim ubiquitin promoter
HA-ZsGreen
8xLacO
qPCR: #1 #2
E
LacI-Piwi
LacI-Panx
LacI-Nxf2
LacI-Nxt1
fold changes in RNA levels relative to LacI-Renilla (normalized to rp49)
fold changes in HA-ZsGreen protein levels relative to LacI-Renilla (normalized to His3)
act5c
ZsGreen#1
ZsGreen#2
HA-ZsGreen
F
OSC DNA tethering ChIP-seq over sensor
H3K9me3 signal density [rpm]
LacI-Renilla
LacI-Piwi
LacI-Panx
LacI-Nxf2
LacI-HP1a
ZsGreen
8xLacO
D. sim pUbi
Hsp27 term.
mappability
1
3,122
G
fold changes in RNA levels relative to LacI-Renilla (normalized to rp49)
fold changes in HA-ZsGreen protein levels relative to LacI-Renilla (normalized to His3)
LacI-Panx-ΔN
LacI-Panx-ΔC
LacI-Nxf2-ΔCargo
LacI-HP1a
act5c
ZsGreen#1
ZsGreen#2
HA-ZsGreen
H
Piwi
Nxf2
Nxt1
Panx
Cargo
NTF2
UBA
Silencing
Egg

Fabry, Ciabrelli, Munafò et al., Figure 4—figure supplement 1